Six Global Biomass Burning Emission Datasets: Inter-comparison and Application in one Global Aerosol Model

Xiaohua Pan[1,2,*] Charles Ichoku[3], Mian Chin[2], Huisheng Bian[4,2], Anton Darmenov[2], Peter Colarco[2], Luke Ellison[5,2], Tom Kucsera[6,2], Arlindo da Silva[2], Jun Wang[7], Tomohiro Oda[6,2], Ge Cui[7]

1. Earth System Science Interdisciplinary Center, University of Maryland, College Park, MD, USA
2. NASA Goddard Space Flight Center, Greenbelt, MD, USA
3. Howard University, Washington DC, USA
4. Joint Center for Earth Systems Technology, University of Maryland Baltimore City, Baltimore, MD, USA
5. Science Systems and Applications, Inc., Lanham, MD, USA
6. Universities Space Research Association, Columbia, MD, USA
7. University of Iowa, College of Engineering, Iowa City, IA, USA

* xpan333@umd.edu

Abstract

Aerosols from biomass burning (BB) emissions are poorly constrained in global and regional models, resulting in a high level of uncertainty in understanding their impacts. In this study, we compared six BB aerosol emission datasets for 2008 globally as well as in 14 sub-regions. The six BB emission datasets are: (1) GFED3.1 (Global Fire Emissions Database version 3.1); (2) GFED4s (GFED version 4 with small fires); (3) FINN1.5 (FIre INventory from NCAR version 1.5); (4) GFAS1.2 (Global Fire Assimilation System version 1.2); (5) FEER1.0 (Fire Energetics and Emissions Research version 1.0), and (6) QFED2.4 (Quick Fire Emissions Dataset version 2.4). The global total emission amounts from these six BB emission datasets differed by a factor of 3.8, ranging from 13.76 to 51.93 Tg for organic carbon and from 1.65 to 5.54 Tg for black carbon. In most of the regions, QFED2.4 and FEER1.0, which are based on the satellite observations of fire radiative power (FRP) and constrained by aerosol optical depth (AOD) data from the Moderate Resolution Imaging Spectroradiometer (MODIS), yielded higher BB emissions than the rest by a factor of 2-4. By comparison, the BB emission estimated from GFED4s and GFED3.1, which are based on satellite burned-area data, but with no AOD constraints, were at the low end of the range. In order to examine the sensitivity of model simulated AOD to the different BB emission datasets, we ingested these six BB emission datasets separately into the same global model, the NASA Goddard Earth Observing System (GEOS) model, and compared the simulated AOD with observed AOD from the AErosol RObotic NETwork (AERONET) and the Multiangle Imaging SpectroRadiometer (MISR) in 14 sub-regions during 2008. In Southern hemisphere Africa (SHAF) and South America (SHSA), where aerosols tend to be clearly dominated by smoke in September, the simulated AOD were underestimated almost in all experiments compared to MISR, except for the QFED2.4 run in SHSA. The model-simulated AOD based on FEER1.0 and QFED2.4 were the closest to the corresponding AERONET data, being, respectively, about 73% and 100% of the AERONET observed AOD at Alta-Floresta in SHSA, and about 49% and 46% at Mongu in SHAF. The simulated AOD based on the other four BB emission datasets accounted for only ~ 50% of the AERONET AOD at Alta Floresta and ~ 20% at Mongu. Overall, during the biomass burning peak seasons, at most of the selected

AERONET sites in each region, the AOD simulated with QFED2.4 were the highest and closest to AERONET and MISR observations, followed closely by FEER1.0. However, the QFED2.4 run tends to overestimate AOD in the region of SHSA, and the QFED2.4 BB emission dataset is tuned with the GEOS model. In contrast, the FEER1.0 BB emission dataset is derived in a more model-independent fashion and is more physical-based since its emission coefficients are independently derived at each grid box. Therefore, we recommend to choose the FEER1.0 BB emission dataset for aerosol-focused hindcast experiments in the two biomass-burning dominated regions in the southern hemisphere, SHAF and SHSA (as well as in other regions but with lower confidence). The differences between these six BB emission datasets are attributable to the approaches and input data used to derive BB emissions, such as whether AOD from satellite observations is used as a constraint, whether the approaches to parameterize the fire activities are based on burned area, FRP, or active fire count, and which set of emission factors is chosen.

1. Introduction

Biomass burning (BB) is estimated to contribute about 62% of the global particulate organic carbon (OC) and 27% of black carbon (BC) emissions annually (Wiedinmyer et al., 2011). Therefore, biomass burning emissions significantly affect air quality by acting as a major source of particulate matter (PM), and the climate system by modulating solar radiation and cloud properties. For instance, a number of studies have revealed that wildfire smoke exposure is harmful to human health by causing general respiratory morbidity and exacerbating asthma, because approximately 80–90% of the smoke particles produced by biomass burning fall within the $PM_{2.5}$ size range (PM with aerodynamic diameter less than 2.5 μm) (Reid et al., 2005, 2016). Moreover, biomass burning emissions have been shown to impact the atmospheric composition in different regions, such as South America (Reddington et al., 2016), Central America (Wang et al., 2006), sub-Saharan African region (Yang et al., 2013), Southeast Asia (Wang et al., 2013; Pan et al., 2018), Indo-China (Zhu et al., 2017), and Western Arctic (Bian et al., 2013). Additionally, BB-produced aerosols can also directly impact the upper troposphere and lower stratosphere via extreme pyro-convection events associated with intense wildfires that generate the storms injecting smoke particles and trace gases into high altitudes (e.g., Peterson et al., 2018). Therefore, emissions from biomass burning constitute a significant component of the climate system, and are crucial inputs required by chemical transport and atmospheric circulation models used to simulate the atmospheric compositions, radiation, and circulation processes needed for air-quality and climate-impact studies (e.g., van Marle et al., 2017).

With the advent of satellite remote sensing of active fire and burned area products in the last couple of decades, a number of global BB emission datasets based on these observations have become available (e.g., Ichoku et al., 2012). Six of such major BB datasets will be compared in this study, including three datasets based on burned area approaches, namely, the Fire INventory from NCAR (FINN, Wiedinmyer et al., 2011) and two versions of the Global Fire Emissions Database (GFED, van der Werf et al., 2006, 2010, 2017), and three datasets based on fire radiative power (FRP) approaches, namely, the Global Fire Assimilation System (GFAS, Kaiser et al., 2012) developed in the European Centre for Medium-Range Weather Forecasts (ECMWF), and two National Aeronautics and Space Administration (NASA) products, i.e., the Fire Energetics and Emissions Research algorithm (FEER, Ichoku and Ellison, 2014) and the Quick Fire Emissions Dataset (QFED, Darmenov and da Silva, 2015).

Although much progress has been made over the last couple of decades in improving the quality of BB emission datasets, for example, by incorporating more recent satellite measurements with better calibration and spatial resolution (e.g., van der Werf et al. 2010; 2017), biomass-burning aerosol emissions still have large uncertainty, and thus are still poorly constrained in models at global and regional levels (e.g., Liousse et al., 2010; Kaiser et al., 2012; Petrenko et al., 2012, 2017; Bond et al., 2013; Zhang et al., 2014; Pan et al., 2015; Ichoku et al., 2016a; Reddington et al., 2016; Pereira et al., 2016). Specifically, large uncertainty exists in the description of the magnitude, patterns, and drivers of wildfires and types of biomass burning (e.g., Hyer et al, 2011). For instance, a global enhancement of particulate matter BB emission by a factor of 3.4 was

recommended for GFAS by Kaiser et al. (2012) to match the observed aerosol loading. Andreae (2019) commented that "In contrast to gaseous compounds, which are chemically well defined, aerosols are complex and variable mixtures of organic and inorganic species and comprise particles across a wide range of sizes. This affects in particular the measurements of organic aerosol, black/elemental carbon, and size fractionated aerosol mass".

A recent analysis with multiple models has been conducted under the auspices of the Aerosol Comparisons between Observations and Models (AeroCom) Phase III biomass burning emission experiments using the GFED version 3.1 (GFED3.1) as input to several models (hereinafter, "The AeroCom multi-model study", https://wiki.met.no/aerocom/phase3-experiments) (Petrenko et al., manuscript in preparation). The AeroCom Multi-model study concluded that the modelled aerosol optical depth (AOD) from different models exhibits large diversity in most regions, i.e. some models overestimate while other models underestimate. However, over two major biomass burning dominated regions, South America and southern hemisphere Africa, all models consistently underestimate AOD. This result suggests that the underestimation of AOD in these two regions was more likely attributable to the GFED3.1 biomass burning emission dataset rather than the model configurations.

Our study aims to explore multiple BB emission datasets, including GFED3.1, GFED version 4 with small fires (GFED4s), FINN version 1.5, GFAS version 1.2, QFED version 2.4, and FEER version 1.0, in order to investigate the discrepancies between these six BB emission datasets by comparing them at both regional and global levels. Such a comparative evaluation of BB emission datasets would show the differences between them as well as how these differences propagate through the physical processes of related aerosols in models, e.g., dry and wet deposition, transport, atmospheric abundance, and the resulting AOD. Our study is expected to provide further insight into the development of possible mitigation for the current large uncertainties in BB emissions. The similar comparative studies of multiple BB aerosol emission datasets have been previously conducted at regional scales, e.g., by Zhang et al. (2014) in the northern sub-Saharan African region, Pereira et al. (2016) in South America, and Reddington et al. (2016) in the entire tropical region. The current study not only provides for the first time a global assessment and analysis of these six BB emission datasets to provide a world-wide perspective, but also examines their performance within 14 regions (Fig. 1). The 14 regions were previously defined for a series GFED-based studies (e.g., Van der Werf et al., 2006, 2010, and 2017).

In the rest of this paper, we first describe these six BB emission datasets, the GEOS model configuration and experimental designs, and observations in Sect. 2, then we show comparisons of the biomass burning emissions datasets and the resulting model simulated AOD in Sect. 3. We discuss possible attributions of the differences between the six BB emission datasets to the sources of uncertainty associated with the biomass burning emissions and the aerosol modeling in Sect. 4. Conclusions and recommendations are presented in Sect. 5.

2. Methodology

2.1 Six BB emission datasets

General information about each of the six biomass burning emission datasets investigated in this study, namely GFED3.1, GFED4s, FINN1.5, GFAS1.2, FEER1.0, and QFED2.4, is given below. Their main attributes, such as their spatial and temporal resolutions, the methods used to estimate burned area (where applicable), the method to derive emission coefficients (where applicable), and the references for the emission factors, are compared in Table 1. Overall, all datasets provide daily global biomass burning emissions since 2003.

2.1.1 GFED3.1

The total dry matter consumed by biomass burning in GFED3.1 (van der Werf et al., 2010) is estimated by the multiplication of the MODIS burned area product at 500-m spatial resolution (Giglio et al. 2010, for the MODIS era) and fuel consumption per unit burned area, the latter being the product of the fuel loads per unit area and combustion completeness. This estimation is conducted using the Carnegie–Ames–Stanford approach (CASA) biogeochemical modeling framework that provides estimates of biomass in various carbon "pools" including leaves, grasses, stems, coarse woody debris, and litter. Fuel loads in CASA are estimated according to carbon input information on vegetation productivity, and carbon outputs through heterotrophic respiration, herbivory, fires, and tree mortality (Giglio et al., 2010; van der Werf et al., 2010). Then, the biomass burning emission of a given species is calculated by multiplying the total consumed dry matter with an emission factor of that species (*EF*, with a unit of g species per kg dry matter burned). The *EF* used in GFED3.1 (and most of the other datasets) is mainly chosen from Andreae and Merlet (2001) and/or Akagi et al. (2011), but may also be obtained from various other sources. The GFED3.1 dataset can be accessed through the link: https://daac.ornl.gov/VEGETATION/guides/global_fire_emissions_v3.1.html.

2.1.2 GFED4s

Compared to GFED3.1, the latest GFED version, GFED4s, has a few significant upgrades as described in detail by van der Werf et al. (2017), including (1) additional burned area associated with small fires which were previously omitted by the burned area product but now are compensated by including the active fires to augment the burned area product MCD64A1 (Giglio et al., 2013; Randerson et al., 2012); (2) a revised fuel consumption parameterization optimized using field observations (e.g., van Leeuwen et al., 2014); (3) partitioning of the extratropical forest category into temperate and boreal forests; (4) further dividing forest into temperate and boreal forest ecosystems and applying different sets of emission factors. Among the existing BB emission datasets, GFED4s has hitherto been the most wildly used by modeling communities, such as the Coupled Model Intercomparison Project phase 6 (CMIP6, Van Marle et al., 2017) and AeroCom phase 3 experiment (https://wiki.met.no/aerocom/phase3-experiments). The link to the GFED4s dataset is http://www.globalfiredata.org.

2.1.3 FINN1.5

The FINN1.5 biomass burning emission dataset is developed from its previous version FINN1 (Wiedinmyer et al., 2011) with several updates. It uses satellite observation of

active fire (with confidence level greater than 20%) and land cover from the MODIS instruments onboard the NASA Terra and Aqua polar orbiting satellites, together with the estimated fuel consumption to derive biomass burning emissions. The burned area in each active fire pixel is assumed as 1 km^2, except for grasslands and savannas where it is assigned a value of 0.75 km^2. The fuel consumption at each fire pixel is estimated according to its generic land use/land cover type (LULC) which is assigned using values updated from Table 2 of Hoelzemann et al. (2004) in the various world regions based on Global Wildland Fire Emission Model (GWEM). With the estimated burned area, fuel consumption, and *EF* of individual species, the daily global open biomass burning emissions of each species are then calculated at a 1 km spatial resolution. The FINN1.5 emissions dataset is archived at: http://bai.acom.ucar.edu/Data/fire/.

2.1.4 GFAS1.2

The GFAS1.2 (Kaiser et al., 2012) estimates biomass burning emission rates by multiplying FRP with the conversion factors (Units: kg species per MJ). The global distribution of FRP observations are obtained from the MODIS instruments onboard the Terra and Aqua satellites and then are assimilated into the GFAS system. The gaps in FRP observations, which are mostly due to cloud cover and spurious FRP observations of volcanoes, gas flares and other industrial activity, are corrected or filtered in the GFAS system. Eight biome-specific conversion factors are calculated by linear regressions between the GFAS FRP and the dry matter combustion rate of GFED3.1 in each biome (see Table 2 and Fig.3 in Kaiser et al., 2012). Therefore, the biomass burning emission calculated by GFAS1.2 is close to that of GFED3.1. Then the biomass burning emission from a certain aerosol species is converted by multiplying the total consumed dry matter with the *EF* of that species. More information on the latest GFAS product can be found at https://confluence.ecmwf.int/display/CKB/CAMS++Global+Fire+Assimilation+System+%28GFAS%29+data+documentation.

2.1.5 FEER1.0

The FEER1.0 (Ichoku and Ellison, 2014) multiplies its emission coefficients C_e (Units: kg species per MJ) with MODIS FRP data that have been preprocessed and gridded in the GFAS1.2 analysis system (Kaiser et al., 2012) to derive aerosol biomass burning emission rates. The C_e in FEER1.0 for smoke aerosol total particulate matter (TPM) is derived through zero-intercept regression of the emission rate of smoke aerosol (i.e., R_{sa}) against the corresponding FRP (Ichoku and Kaufman, 2005; Ichoku and Ellison, 2014) at pixel-level within each grid. C_e corresponds to the slope of the linear regression fitting. In the FEER methodology, R_{sa} is estimated through a spatio-temporal analysis of MODIS AOD data along with wind fields from the NASA Modern-Era Retrospective Analysis for Research and Applications (MERRA) reanalysis dataset (Rienecker et al., 2011). The smoke aerosol C_e in FEER1.0 is available at 1°×1° spatial resolution global grid, and covers most of the land areas where fires have been detected by MODIS for at least 30 times during the period 2003-2010 (Ichoku and Ellison, 2014) to ensure statistical representativeness. In the current version of FEER1.0 emission dataset, C_e for other smoke constituents, say OC, at each grid cell are obtained by scaling the C_e of smoke aerosol according to the ratio of their emission factors, such as EF_{oc} *to* EF_{sa} (i.e., ratio of

emission factor for OC to that for total smoke aerosol). The FEER1.0 dataset is available at http://feer.gsfc.nasa.gov/data/emissions/.

2.1.6 QFED2.4

The earlier version of QFED (Darmenov and da Silva 2015) estimated biomass burning emissions by multiplying level 2 MODIS FRP with an emission coefficient C_e which is the product of the initial constant value C_0 (1.37 kg per MJ, reported by Kaiser et al., 2009) and a scaling factor, with the scaling factor calculated by regressing the carbon monoxide (CO) BB emission (product of FRP, C_0 and CO emission factor) to that in the GFED version 2. The scaling factor used by the QFED 2.4, the version used in this study, was obtained by further regressing the Goddard Earth Observing System (GEOS) Model simulated AOD to the MODIS AOD in 46 sub-regions, and then the resulting scaling factors in the 46 sub-regions were aggregated into four major fire-prone biomes, i.e., savanna, grassland, tropical forests, and extratropical forests, as values of 1.8, 1.8, 2.5, and 4.5, respectively. The QFED2.4 also used a sequential model with temporally damped emissions to estimate the emissions in cloudy areas. The real-time QFED2.4 fire emission is produced on a daily basis and used in the operational GEOS data assimilation system. In addition to the near real-time emissions, a longer historical record dataset, which is what we have used, is stored at https://portal.nccs.nasa.gov/datashare/iesa/aerosol/emissions/QFED/v2.4r6/.

2.2 Application of the BB emission datasets in the NASA GEOS model

2.2.1 Description of the NASA GEOS model

The GEOS model consists of an atmospheric general circulation model, a catchment-based land surface model, and an ocean model, all coupled together using the Earth System Modeling Framework (ESMF, Rienecker et al., 2011; Molod et al., 2015). Within the GEOS model architecture, several interactively coupled atmospheric constituent modules have been incorporated, including an aerosol and carbon monoxide (CO) module based on the Goddard Chemistry Aerosol Radiation and Transport model (GOCART, Chin et al., 2000, 2002, 2009, 2014; Colarco et al., 2010; Bian et al., 2010) and a radiation module from the Goddard radiative transfer model (Chou and Suarez, 1999; Chou et al., 2001). The GOCART module used in this study includes representations of dust, sea salt, sulfate, nitrate, and black and organic carbon aerosol species. A conversion factor of 1.4 is used to scale organic carbon mass to organic aerosol (OA), which is on the low end of current estimates (Simon and Bhave, 2012).

In this study the GEOS model (Heracles-5.2 version) was run globally on a cubed-sphere horizontal grid (c180, ~50 km resolution) and with 72 vertical hybrid-sigma levels extending from the surface to ~85 km for the year 2008. The model was run in a "replay" mode, where the winds, pressure, moisture, and temperature are constrained by the MERRA-2 reanalysis meteorological data (Gelaro et al., 2017), a configuration that allows a similar simulation of real events as in a traditional off-line chemistry transport model (CTM) but exercises the full model physics for, e.g., radiation, and moist physics processes. We used the HTAP2 anthropogenic emissions (Janssens-Maenhout et al., 2015) that provides high-spatial resolution monthly emissions. The BB emissions are

uniformly distributed within the boundary layer without considering the specific injection height of each plume. All six BB emissions are daily emissions with the diurnal cycle prescribed in the model: the maximum is around local noon, which is more prominent in the tropics, and is gradually weakened in the extra-tropics (Randles et al., 2017). The natural aerosols are either generated by the model itself (i.e., wind-blown dust and sea salt) or from prescribed emission files (i.e., volcanic and biogenic aerosols).

2.2.2 Experiment design

In order to investigate the sensitivity of the modelled AOD to different BB emission datasets, seven experiments were conducted with the GEOS model, differing only in the source of biomass burning emissions. The first six runs are GFED3.1, GFED4s, FINN1.5, GFAS1.2, FEER1.0, and QFED2.4, using the corresponding biomass burning datasets described above in Section 2.1. A seventh run is called "NOBB," where the model is run without including biomass burning emissions.

2.4. AOD Observations

2.4.1 MISR retrievals

We evaluated the simulated monthly AOD with the half-degree monthly level 3 Multiangle Imaging SpectroRadiometer version 23 (MISR v23, with the filename tagged as F15_0032) total AOD data at 558 nm wavelength on board the EOS-Terra satellite (Kalashnikova and Kahn, 2006; Kahn et al., 2010). The data can be downloaded from the website: https://eosweb.larc.nasa.gov/project/misr/mil3mae_table.

2.4.2 AERONET sites

We also evaluated the modelled 3 hourly and monthly AOD at 550nm and Angström Exponent (AE, 440–870 nm) with that from the ground-based AErosol RObotic NETwork (AERONET, Holben et al., 1998) sites situated in biomass burning source regions. AERONET Version 3 Level 2.0 data, which are cloud-screened and quality-assured aerosol products with a 0.01 uncertainty (Giles et al., 2019), were used in this study. The data can be downloaded from the websites: https://aeronet.gsfc.nasa.gov/new_web/download_all_v3_aod.html. The AERONET AOD at 550nm is interpolated from the measurements at 440 and 675nm. AE is calculated with AOD at 440 and 870nm. We compared model simulations with AERONET data at 14 selected sites, each representing the spatiotemporal characteristics at different biomass burning regions shown in Fig. 1. The 14 regions are defined previously by the GFED studies (e.g., Van der Werf et al., 2006, 2010, and 2017). Since some regions, such as Northern Hemisphere South America (NHSA) and Equatorial Asia (EQAS), have no AERONET sites with data measured in 2008, we also used the average of multiple years or climatology of AERONET AOD at each site for reference. Locations of these 14 selected AERONET sites are represented by the numbered magenta dots in Fig.1.

3. Results

3.1 Inter-comparison of the six biomass burning emission datasets

The biomass burning OC emissions were compared throughout this study, since OC is the major constituent in fresh biomass burning smoke particles, with mass fractions ranging

from 37% to 67% subject to fuel type (e.g., grassland/savanna, forests, or others), according to various studies based on thermal evolution techniques (Reid et al., 2005, part II, Table 2). These inter-comparisons were carried out in terms of both annual and seasonal variations in Sect. 3.1.1 and Sect. 3.1.2, respectively.

3.1.1 Annual total

Figure 2 shows the spatial distributions of annual total biomass burning OC emissions in 2008 from the six BB emission datasets. The regions with high emission of OC in Africa, boreal Asia, and South America were pronounced in all six BB emission datasets, albeit to different degrees. The regional differences of the annual total biomass burning OC emissions in different BB emission datasets can be appreciated more quantitatively in Fig. 3. Relevant statistics for the six BB emission datasets in the 14 regions are also listed at the top of the panel in Fig. 3, with the mean averaged over the six BB emission datasets in the first row (*mean*). We used three different measures to quantify the spread of the annual total from the six BB emission datasets: (1) standard deviation (*std*), (2) ratio of maximum to minimum (*max/min*), and (3) the coefficient of variation (*cv*, defined as the ratio of the *std* to the *mean*). The rank of *cv* for each of the 14 regions is also listed in Fig. 3 (e.g., a ranking of 1 means that this region shows the least spread among the six BB emission datasets, while a ranking of 14 indicates that this region has the largest spread). The best agreements among the six emission datasets occurred in Northern Hemisphere Africa (NHAF), Equatorial Asia (EQAS), Southern Hemisphere Africa (SHAF), and Southern Hemisphere South America (SHSA), which have the top *cv* ranks (1-4) and relatively low *max/min* ratio (a factor of 3-4). The worst agreements occurred in the Middle East (MIDE), Temperate North America (TENA), Boreal North America (BONA) and Europe (EURO), which have the bottom *cv* ranks (14-11) and large *max/min* ratio (a factor of 66-10). This diversity was mostly driven by the QFED2.4 emission dataset, which estimated the largest emission amount for almost all regions (except EQAS), especially in MIDE where the BB emission from QFED2.4 is more than 50 times higher than those from the two GFED versions. Globally, the QFED2.4 dataset showed the highest OC emission of 51.93 Tg C in 2008, which was nearly four times that of GFED4s at 13.76 Tg C (the lowest among the six BB datasets).

Overall, two FRP-based BB emissions, QFED2.4 and FEER1.0, were a factor of 2-4 larger than the other BB datasets. This result is consistent with the findings of Zhang et al. (2014) over sub-Saharan Africa. It is worth noting that the BB emission amount of GFAS1.2 was close to that of GFED3.1, reflecting the fact that GFAS1.2 is tuned to GFED3.1(described in Sect. 2.1.4). Globally, FINN1.5 yielded more OC emissions than the two GFED and GFAS1.2 datasets (e.g., 40% larger than GFED4s). Regionally, FINN1.5 was generally comparable to the two GFED datasets in most of the regions, but was higher than them in the tropical regions, such as EQAS, Southeast Asia (SEAS), Central America (CEAM) and Northern Hemisphere South America (NHSA). Interestingly, FINN1.5 was even the largest among all six datasets over the EQAS region, which might be associated with its assumption of continuation of burning into the second day in that region (to be discussed in section 4.1.2). The global OC emissions from GFED4s were lower than those from its GFED3.1 counterpart, although higher in several other regions, such as TENA, CEAM, NHSA, Boreal Asia (BOAS) and Central Asia

(CEAS). Possible explanations for these differences among the six global BB emissions datasets are provided in Sect. 4.1.

3.1.2 Seasonal variation

Biomass burning is generally characterized by distinct seasonal variations in each of the 14 regions and globally, as shown in Fig. 4. Overall, there were four peak fire seasons across the regions: (1) During the boreal spring (March-April-May), fires peak in BOAS mainly because of forest fires (see the contribution of different fire categories in Table 3 of van der Werf et al., 2017), in CEAM, NHSA, and SEAS because of savanna and deforestation fires, and in Central Asia (CEAS) mainly due to the agricultural waste burning to prepare the fields for spring crops. (2) During the boreal summer (June-July-August), fires peak in BONA and TENA, mostly due to wildfires that occur under the prevailing dry and hot weather, in EURO probably associated with the burning of agricultural waste. In addition, we found that fire peaked in MIDE in three FRP-based datasets, i.e., QFED2.4, FEER1.0 and GFAS1.2. It might be associated with the failure to filter out the gas flares from the FRP fire product, in particular in QFED2.4 (Darmenov and da Silva 2015). (3) During the austral spring (September-October-November), fires peak in the southern hemispheric regions of SHSA, SHAF and AUST, associated with savanna burning (in addition to deforestation fires in SHSA). In SHSA, two GFED versions peaked in August, one month early than the rest; (4) During the boreal winter (December and January), fires peak in NHAF, particularly along the sub-Sahel belt (Fig. 2), where savanna fires are associated with agricultural management and pastoral practices across that region (e.g., Ichoku et al., 2016b). Overall, all six BB emission datasets exhibited similar seasonal variations, although they differed in magnitude. In particular, it is noteworthy that in EQAS, the annual OC emissions from GFED4s was lower than that of GFED3.1 by 18%, but higher by a factor of two in the month of August when peatland burning is predominant.

For reference, biomass burning black carbon (BC) emissions were also shown, but in the supplement (Fig. S1, S2 for annual total and Fig. S3 for seasonal variation), which exhibited similar features as OC. The amounts of biomass burning BC emission were almost proportional to their OC counterparts (about 1/10 to 1/15 of OC).

3.2 Comparison of model-simulated AOD with remote sensing data

As in other similar situations where several different datasets are available to be chosen from (e.g. Bian et al., 2007), a question that invariably comes to mind is: which BB emission dataset is the most accurate or should be used in a given situation? In fact, it is difficult to give a conclusive answer, as it is often challenging to measure the emission rate of an active fire in real time or to disentangle the contribution of smoke aerosols from the total atmospheric aerosol loading/concentration in observations. Therefore, in this study we have implemented all six global BB emission datasets separately in the GEOS model, and evaluated their respective simulated aerosol loadings. More specifically, we compared the simulated AOD with the satellite-retrieved AOD data from MISR (primarily to examine the spatial coverage) as well as with ground-based measurements from AERONET sites near biomass burning source regions to examine the seasonal variation. Our analysis was focused on the regional biomass burning peak

seasons, when smoke aerosol emissions dominate those from other sources, such as pollution or dust. With such an effort to evaluate the sensitivity of the simulated AOD to the different BB emission datasets, the results from this study may shed some light on answering the aforementioned question, i.e., which BB dataset is the most accurate or should be used in a given situation? We acknowledge that although the result from a particular model (e.g., GEOS in this case) can potentially introduce additional uncertainty through various complicated and non-linear procedures employed to calculate the AOD, such as the modelled relative humidity and the related aerosol's hydroscopic growth (Bian et al., 2009; Pan et al., 2015), still, evaluation of the model-simulated AOD has proven to be a feasible approach to compare various BB emission datasets in reference to the currently available observations (e.g., Petrenko et al. 2012; Zhang et al., 2014).

Aiming to evaluate the sensitivity of the modelled AOD to different BB emissions datasets, we compared the spatial distribution of the GEOS model-simulated AOD with MISR-retrieved AOD in Sect. 3.2.1 and with the AERONET measured AOD at 14 AERONET sites in Sect. 3.2.2. We also conducted an in-depth study at two AERONET sites, Alta Floresta (in the southern hemisphere South America, SHSA) and Mongu (in the southern hemisphere Africa, SHAF), as discussed in Sect. 3.3.

3.2.1 Global spatial distribution

Comparisons for September and April in 2018 are shown in Fig. 5 and Fig. 6 respectively, representing the peak biomass burning months in the southern hemisphere, and many regions in the northern hemisphere, respectively. The MISR AOD is displayed on the top left panel and the model biases (model minus MISR) from seven individual experiments are shown on the rest of panels.

In September 2008, the high AOD observed from MISR (Fig. 5a) in the southern hemisphere was mostly attributable to biomass burning. A large fraction of the southern hemisphere Africa (SHAF) were featured with high AOD (greater than 0.5). The area-averaged AOD over the entire SHAF was 0.331 (see Table S1 for the area-averaged MISR AOD in each region). The observed AOD peaked in the southern Congo (nearly 1.0) and gradually decreased westwards. Large negative model bias (-0.283) was found in the NOBB run over the region of SHAF (greenish shading in Fig. 5b; see Table S1 for the area-averaged model biases in each region). The negative bias was reduced most significantly in the QFED2.4 run (see Fig. 5h), to -0.044, followed by the FEER1.0 run (see Fig. 5g), to -0.079, but the least in GFED4s and GFAS1.2 (see Fig. 5d and f, respectively), still as large as -0.208.

In the southern hemisphere South America (SHSA), where the area-averaged MISR AOD was 0.188, the maximum AOD was ~0.7 in the central Brazil (Fig. 5a). The negative bias averaged over SHSA was a value of -0.132 in the NOBB run (Fig. 5b). It was reduced most significantly in the FEER1.0 run to -0.021 (Fig. 5g), but overcorrected in the QFED2.4 run to 0.020 (see reddish shading in Fig. 5h). The reduction of negative bias was the least again in the GFED4s run (Fig. 5d) and the GFAS1.2 run (Fig. 5f), still as large as -0.081 and -0.080, respectively.

Being mixed with and often surpassed by other aerosol types, however, the contribution of biomass burning aerosols to the total AOD is hardly distinguishable from those of other sources in the peak months in certain regions, such as April (Fig. 6) in the regions of Southeast Asia (SEAS), Central Asia (CEAS), and Boreal Asia (BOAS). Such complicated situations lead to the difficulties in evaluating the BB emission datasets with the AOD observations, in particular when the background AOD represented by the NOBB run was already overestimated in latter two regions.

3.2.2 Seasonal variations of AOD at AERONET sites

In order to better quantify the sensitivity of the simulated AOD to the six different BB emission datasets, we further compared the simulated monthly AOD with the ground-based AOD observations from AERONET stations by choosing one representative station in each region (see Fig. 7, and the panels representing the AERONET stations in Fig. 7 were arranged in a way that their placements correspond to those of their respective regions in Fig. 4 for easy reference). The exception is in two regions NHSA and EQAS, where there are no valid AERONET observations during 2008. Thus, we used the multi-year climatology of AOD at Medellin and Palangkaraya to represent NHSA and EQAS, respectively. We also included the climatology of AERONET AOD in the other 12 AERONET sites for reference. As shown in Fig. 7, the annual cycle of AOD in 2008 at available sites (brown thin bars) were similar to their respective climatology (light gray thick bars) to within 0.05. The MISR AOD was plotted for reference as green diamond. In this section, the modelled monthly mean AOD was calculated by averaging over the modelled instantaneous AOD in each month; while the monthly AOD of AERONET and MISR are simply calculated by averaging over available observations in each month.

Contributions from non-BB emissions to the total AOD are represented by NOBB experiment (black line in Fig. 7). Runs with different BB emission datasets showed almost identical AOD during non-biomass burning seasons at each selected AERONET station in each region, thereby allowing their differences to be noticeable during the biomass burning peak seasons. At Alta Floresta in Brazil (Fig. 7.5), Mongu in Zambia (Fig. 7.9), and Chiang Mai Met Sta in Thailand (Fig. 7.12), where the biomass burning emissions dominated the peak AOD, almost all experiments underestimated AOD during the respective peak biomass burning seasons. However, the fact is that the contribution of non-BB AOD was usually more than that of BB AOD during the burning seasons at most of the selected AERONET sites, except at three sites above, Therefore, it is difficult to disentangle the effect of biomass burning on the total AOD in most situations, especially when the model has difficulty representing the non-BB AOD, leading, for example, to overestimation at three high-latitude (> 55°N) AERONET sites (the three panels in the top row of Fig. 7), i.e., Fort McMurray in Canada (Fig. 7.1), Toravere in Estonia (Fig. 7.6), and Moscow_MSU_MO in Russia (Fig. 7.10). However, it is apparent that the simulated AOD with QFED2.4 were overestimated during October and November at Fort McMurray in USA, indicating that QFED2.4 overestimated BB organic carbon emission during these two months. In general, at most of AERONET sites, the simulated AOD based on QFED2.4 were the highest and closest to AERONET AOD during the

corresponding peak of the biomass burning seasons, followed by FEER1.0 and FINN1.5, and then GFED3.1, GFEDv4 and GFAS1.2.

3.3 Case studies in biomass burning dominated regions

In order to investigate the relationship between AOD and biomass burning emission in the context of daily variation, we focused on two AERONET stations, namely, Alta Floresta in Brazil and Mongu in Zambia during September, for the in-depth analysis in this section. Biomass burning emissions are known to be dominant at such locations and month as estimated by Chin et al. (2009), who found that 50-90% of the AOD was attributable to biomass burning emissions according to GOCART model simulations. Based on other previous studies also, e.g., Pereira et al. (2016) in southern hemisphere South America, Reddington et al. (2016) in tropical regions including southern hemisphere South America and Africa, and the AeroCom Multi-model study lead by Dr. Petrenko mentioned earlier in the introduction part, there appears to be a general consensus that the simulated AOD is consistently underestimated over southern hemisphere South America and Africa in many models with different BB emission datasets. In this study, we calculated the 3-hourly AOD by sorting the instantaneous AOD from both AERONET and model outputs for each day into eight time-steps, namely, 0, 3, 6, 9, 12, 15, 18, and 21Z. The modelled monthly mean AOD was calculated by averaging over the modelled 3-hourly AOD, which coincided with 3-hourly AERONET AOD in that month. The detailed analyses are discussed below.

3.3.1 Alta Floresta in Brazil (Southern Hemisphere South America)

The monthly averaged AOD observed from AERONET at Alta Floresta is 0.47 during September 2008 (Fig. 8a). It shows that the simulated AOD from all six experiments captured the sustained aerosol episode observed in the AERONET dataset during September 13-14 (AOD about 1.0-1.5). The simulation with QFED2.4 BB emission produced the closest agreement with the AERONET-observed AOD with an average *ratio* of 1.00. In contrast, the simulated AOD with FEER1.0 (*ratio*=0.73), FINN1.5 (*ratio*=0.55), GFAS1.2 (*ratio*=0.42), GFED3.1(*ratio*=0.40), and GFED4s (*ratio*=0.36) tended to underestimate for most of the time. All experiments showed relatively low skill of capturing the temporal variability of the observed AOD at Alta Floresta (*corr*=0.24-0.60). The Angström Exponent (AE: an indicator of particle size) from AERONET is 1.66 (not shown), indicating that small particles, most likely those from smokes, dominated the total aerosol loading at Alta Floresta (Eck et al., 2001). All experiments matched the observed AE (not shown).

The OC column mass loading (Fig. 8b) resembled the corresponding AOD (Fig. 8a), implying that the day-to-day variation of OC column mass loading in this dry season dominates the change of AOD in the model, rather than other factors such as relative humidity (RH). The OC column mass loading is determined by the regional scale of emission, transport, and removal processes of aerosols, the latter two processes of which are the same across the six experiments given the same model configurations were used. Therefore, the differences of OC column mass loading and thus AOD across the six experiments are attributed to the different choices of biomass burning emission datasets. Figure 8c shows the local biomass burning OC emissions in different biomass burning

emission datasets (i.e., at the 0.5°×0.5°grid box where this site is located). We found that there was a large contrast in the local biomass burning OC emission between September 24-25 (as high as 1-2 $\mu g\ m^{-2}\ s^{-1}$) and the other days (close to zero) across the six experiments, in spite of the differences in magnitude. Similar emission patterns are found when averaged over nine or 25 surrounding grid boxes (not shown). Such sharp contrast was completely absent in the simulated OC column mass density (Fig. 8b) and AOD (Fig. 8a).

All of this evidence, therefore, collectively suggest that the temporal variations of AOD (and aerosol mass loading) in Alta Floresta during the burning season do not directly respond to the local BB emission at the daily and sub-daily time scales, but to the regional emission. The regional emission is adjusted by the processes determining the residence time of aerosols (typically a few days), such as the regional scale transport and removal of aerosols. The MODIS-Terra true color image overlaid with active fire detections (red dots) on September 13, 2008 (Fig. 8d) confirms that there were no active fires (represented by red dots) detected at Alta Floresta (blue circle), and thus the dense smoke over there was transported from the upwind areas instead from local BB emissions during this peak aerosol episode. Therefore, accurate estimation of both the magnitude and spatial pattern of regional emissions are rather important.

3.3.2 Mongu in Zambia (Southern Hemisphere Africa)

The case at Mongu is different from that at Alta Floresta. There were numerous active fire detections (represented by the red dots in this MODIS-Aqua true color image) at and close to Mongu (blue circle), as revealed by Fig. 9d on September 12, 2008, one of peak aerosol episodes. The visibility over the entire region was apparently low due to smoke aerosols. Figure 9a shows that the simulated AOD from all six experiments captured two peak aerosol episodes observed from the AERONET dataset during September 2-3 and September 11-12 (AOD about 1.0), albeit underestimated. But all experiments failed to capture the sustained aerosol episode after September 20 (the observed AOD is about 0.5). All model experiments almost reproduced the AERONET AE value of 1.80 throughout September at this site (not shown), confirming that the dominance of the fine-mode aerosol particles in smoke aerosols is captured by the model irrespective of the BB emission dataset used.

The biomass burning OC emissions averaged over the grid box of Mongu exhibited distinct daily variations in each BB dataset (Fig. 9c). Similar emission patterns are found when averaged over nine or 25 surrounding grid boxes (not shown). At this site, the day-to-day variations of AOD still cannot be totally explained by the corresponding local emission at Mongu. For example, emission from FEER1.0 on September 17 is six times higher than that on September 2 (Fig. 9c), but the simulated AOD on September 17 is twice lower than that on September 2 (Fig. 9a). However, the magnitude of AOD at Mongu in each experiment corresponded to the magnitude of BB emission at the regional scale, since it is apparent that overall higher regional BB emissions still resulted in higher column mass loading and thus AOD. For instance, FEER1.0 and QFED2.4, which have the largest monthly total biomass burning OC emission over the region of SHAF among the six BB emission datasets during September (2.27 and 2.92 Tg mon^{-1}, respectively, as

shown in Fig. 4), corresponded to the highest AOD (*ratio*=49% and 46%, respectively, as shown in Fig. 9a); while FINN1.5 and GFED4s, which represent the lowest monthly mean biomass burning OC emission over the region of SHAF (0.87 and 0.85 Tg mon^{-1}, respectively, as shown in Fig.4), corresponded to very low AOD (15% and 19% of the observed, respectively).

Although the temporal variation of the ambient RH may partially contribute to the day-to-day changes of the emission-AOD relationship, the close resemblance between the model simulated AOD and column OC mass loading (Fig. 9b) excludes such possibility. This evidence therefore suggest again that the temporal variations of AOD (and aerosol mass loading) in Mongu, where local emissions were present, do not also directly respond to the local BB emission at the daily and sub-daily time scales during the burning season, further confirming the importance of accurate estimation of both the magnitude and spatial pattern of regional emissions as mentioned in the case of Alta Floresta. Therefore, over southern hemisphere Africa and southern hemisphere South America, except for QFED2.4, enhancement of regional BB emission amounts in all the other BB emission datasets (although to different degrees) is suggested by this study in order to reproduce the observed AOD level.

4. Discussion

The simulated AOD is biased low in biomass burning dominated regions and seasons across all six BB emission datasets as demonstrated in this study. More explanations on differences among the six BB emissions datasets are discussed in Sect. 4.1. Basically, the uncertainty of the simulated AOD could be attributable to two main sources: (1) BB emissions-related biases; (2) Model-related biases. They are discussed in Sections 4.2 and 4.3, respectively.

4.1 The possible explanations of differences among the six BB emission datasets

4.1.1 Higher BB emissions estimated from QFED2.4 and FEER1.0

This study has shown that the QFED2.4 and FEER1.0 BB emission datasets are consistently higher than the others, with QFED2.4 being the highest overall. Some of the possible reasons responsible for this difference include:

Constraining with MODIS AOD. The emission coefficients (C_e) used to derive biomass burning emissions in both QFED2.4 and FEER1.0 are constrained by the MODIS AOD, although in different ways (detailed in Sec.2.1.6 and 2.1.5, respectively). This is not the case for other BB emission datasets, especially GFAS1.2, although it also uses the same FRP products as FEER1.0 in deriving dry mass combustion rate (it is tuned to that of GFED3.1 instead). QFED2.4 applied four biome-dependent scaling factors to the initial constant value C_0 when deriving its C_e, by minimizing the discrepancy between the AOD simulated by the GEOS model and that from MODIS in the respective biomes. The resulting QFED2.4 scaling factors are 1.8 for savanna and grassland fires, 2.5 for tropical forests, and 4.5 for extratropical forests (Darmenov and da Silva 2015). This partially explains its very high emission over the extratropical regions of TENA, BONA and BOAS relative to the other emission datasets (Fig. 2-4). However, the high BB emission estimated by QFED2.4 is questionable during October and November of 2008 in the

region of BONA (Fig. 4) according to the evaluation of its resulting AOD relative to the AERONET AOD at the Fort McMurray site (Fig. 7.1). As for FEER1.0, the process of deriving C_e involved calculating the near-source smoke-aerosol column mass with the MODIS AOD (total minus the background) for individual plumes, thereby limiting influence from other emission sources (Ichoku and Ellison, 2014).

Fuel consumption. In general, the FRP-based estimation approaches, such as GFAS1.2, QFED2.4, and FEER1.0, may enable more direct estimates of fuel consumption from energy released from fires, without being affected by the uncertainties associated with the estimates of fuel loads and combustion completeness (e.g., Kaufman et al., 1998; Wooster et al., 2003, 2005; Ichoku and Kaufman, 2005; Ichoku et al., 2008; Jordan et al., 2008). However, FRP from non-BB sources, such as the gas flare, could be mistakenly identified as BB sources. One example is over bare land in the eastern border of Algeria in MIDE (refer the land type to the website: http://maps.elie.ucl.ac.be/CCI/viewer/index.php) by QFED2.4 (see Fig. 2f), thus additional screening of FRP fire product is required.

4.1.2 Features of FINN1.5

Globally, the FINN1.5 dataset is lower than QFED2.4 and FEER1.0, but larger than GFAS1.2, GFED3.1 and GFED4s (Fig. 3). Although FINN1.5 can capture the location of the large wildfires using the active fire products, the estimation of burned area is rather simple without the complicated spatial and temporal variability in the amount of burned area per active fire detection or variability in fuel consumption within biomes. For example, it estimates 1 km^2 burned area per fire pixel for all biomass types except for savanna and grassland where 0.75 km^2/fire pixel is estimated instead. That might partially explain why the FINN1.5 is extremely low in AUST, as suggested by Wiedinmyer et al. (2011). Additionally, the FINN1.5 dataset is the least over boreal regions, such as in regions of BOAS and BONA, where FINN1.5 is only 1/3 and 3/5 of GFED4s, respectively. Large forest fires dominate in BOAS and BONA, such that the direct mapping of burned area as done in GFED4s and GFED3.1 produces more biomass burning emissions (van der Werf et al., 2017). On the other hand, the BB emission in FINN1.5 dataset is relatively large near the equator. For instance, it is the largest among the six datasets over the region EQAS, and the second largest over the regions of CEAM and SEAS (see Fig. 3). This might be attributed to the smoothing of the fire detections in these tropical regions to compensate for the limited daily coverage by the MODIS instruments due to gaps between adjacent swaths and higher chances of cloud coverage in tropical regions (Wiedinmyer et al., 2011). Thus, in FINN1.5, each fire detected in the equatorial region only is counted for a 2-day period by assuming that fire continues into the next day but at half of its original size.

4.1.3 Difference between GFED4s and GFED3.1

Globally and in some regions, biomass burning OC emission in GFED4s is lower than that in GFED3.1 (see Fig. 2-4), although the former has 11% higher global carbon emissions and includes small fires. There are a few possible reasons: 1) For aerosols, the implementation of lower *EF* for certain biomes in GFED4s than in GFED3.1 reduces the aerosol biomass burning emissions. As for the savanna and grassland, for instance, the

GFED4s dataset mainly applies *EF* value recommended by Akagi et al. (2011), which is 2.62 g OC per kg dry matter burned, 18% lower than the *EF* from Andreae and Merlet (2001) used in GFED3.1, which is 3.21 g OC per kg dry matter burned (see Table 2). The new estimation of *EF* is 3.0±1.5 g OC per kg dry matter burned as suggested by Andreae (2019). With it, the OC emissions in savanna and grassland can be slightly enhanced, but would still be lower than those in GFED3.1; 2) In addition, the improvement in including small fires in GFED4s over GFED3.1 is offset by the occasional optimization of fuel consumption using field observations for overall carbon emissions. For instance, the turnover rates of herbaceous leaf (e.g., savanna) are increased in GFED4s, leading to the lower fuel loading and thus lower consumption for this land-cover type in GFED4s (van Leeuwen et al., 2014; van der Werf et al., 2017). Therefore, the biomass burning OC emissions are lower in GFED4s over SHAF, NHAF, and AUST (Fig. 3 and 4), where ~88% of carbon emission is from savanna and grassland (van der Werf et al., 2017).

On the other hand, there are regions in the northern hemisphere where GFED4s is higher than GFED3.1, for example, over CEAS and EURO, where small fires associated with burning of agricultural residues contribute to 43.6% and 58.6% of the carbon emissions, respectively (van der Werf et al., 2017). In spite of the 30% reduction of the *EF* in these two regions, the effect of including small fires in GFED4s is greater, resulting in the biomass burning OC emission from GFED4s being twice as high as that from GFED3.1. Another example is in BOAS where the biomass burning OC emissions are 10% higher in GFED4s than in GFED3.1. This is likely attributable to the higher *EF* used in the former BB dataset than in the latter one for boreal forest fires (9.60 vs. 9.14 g OC per kg dry matter, see Table 2), where 86.5 % of the carbon emission is from the Siberian forest (van der Werf et al., 2017).

It is interesting that the yearly total biomass burning OC emission from GFED4s is 20% lower than that from GFED3.1 in EQAS (Fig. 4), even though the small fires are included and the *EF* of peatland and tropical forest are higher in the former (Table 2). By examining the monthly variations over EQAS (Fig. 4), however, we found that GFED4s is actually higher than GFED3.1 in August by a factor of two when peatland burning is predominant, but equal to or lower than GFED3.1 in other months, particularly in May, leading to the overall lower annual total value in GFED4s.

4.2 Sources of the uncertainty associated with biomass burning emissions

Uncertainty in any of the six BB emissions datasets considered in this study could have been introduced from a variety of measurement and/or analysis procedures, including: detection of fire or area burned, retrieval of FRP, emission factors (see Table 1), land cover maps, and fuel consumption estimates, some of which are explained in detail below.

Fire detection. Most of the current global estimations of biomass burning emissions are heavily dependent on polar-orbiting satellite measurements from MODIS on Terra and Aqua (e.g., MCD14DL, MOD14A1, MYD14A1, and MCD14ML as listed in Table 1). The temporal and spatial resolutions of these measurements impose limitations on their ability to detect and characterize the relevant attributes of fires, such as the locations and timing of active fires and the extent of the burned areas. Each of the two MODIS sensors,

from which all of the major BB datasets derive their inputs, can only possibly observe a given fire location twice in 24 hours, which leaves excessive sampling gaps in the diurnal cycle of fire activity (Saide et al., 2015). Even for these few times that MODIS makes observations at its nominal spatial resolution of 1 km at nadir, it has the potential to miss a significant number of smaller fires (e.g. Hawbaker et al., 2008, Burling et al, 2011, Yokelson et al., 2011), as well as to miss fires obstructed by clouds, those located in the gaps between MODIS swaths in the tropics (Hyer et al., 2009; Wang et al., 2018). In addition, MODIS fire detection sensitivity is reduced at MODIS off nadir views, with increasing view zenith angles especially toward the edge of scan, where its ground pixel size is almost a factor of 10 larger (Peterson and Wang, 2013; Roberts et al., 2009; Wang et al., 2018), resulting in dramatic decreases in the total number of detected fire pixels and total FRP (Ichoku et al., 2016b; Wang et al., 2018). Moreover, all operational remote sensing fire products have difficulty accounting for understory fires or fires with low thermal signal or peatland fires such as those in Indonesia, where smoldering can last for months (Tansey et al, 2008). These issues can propagate into the uncertainties of the emissions datasets that are dependent on active fire detection products, especially those based on FRP, e.g., GFAS1.2 (Kaiser et al., 2012), FEER1.0 (Ichoku and Ellison, 2014), and QFED2.4 (Darmenov and da Silva, 2015). This issue also affects FINN1.5 (Wiedinmyer et al., 2011), which derives the burned area by assuming each active fire pixel to correspond to a burned area of 1 km^2 for most biome types (see details in *Sect.* 2.1.3), and GFED4s, which uses burned area product for large fires but derives burned areas for small fires using the MODIS active fire product.

On the other hand, although the sparse diurnal sampling frequency may not necessarily be an issue for the MODIS burned area product, upon which some of the emission datasets are based (*e.g.*, GFED3.1), burned area product may not account for small fires due to its low spatial resolution of 500-m, which may limit the identification of small burned scars such as those generated by small fires from crop lands (fire size < 21 ha). In addition, the estimation of biomass burning emission based on the burned area product, e.g., GFED, is subject to the uncertainty associated with the estimation of fuel load and combustion completeness as mentioned earlier.

Emission factor (EF). The *EF*, used for deriving individual particulate or gaseous species of smoke emissions from burned dry matter in all major BB emission datasets, heavily depends on the two papers by Andreae and Merlet (2001) and Akagi et al. (2011). The authors of these two studies made significant contributions by compiling the values of *EFs* from hundreds of papers. However, the EFs can have significant uncertainties (Andreae, 2019), because each EF results from a particular experiment or field campaign. Some *EF*s are derived from lab-based studies whereby samples of fuels are burned in combustion chambers (e.g., Christian et al., 2003; Freeborn et al., 2008), where the combustion characteristics can be very different from those of large-scale open biomass burning and wildfires; and some *EFs* are derived from field campaigns, where the measurement locations are often not close enough to the biomass burning source due to personnel safety and other logistic factors (Aurell et al., 2019).

It is somewhat surprising that the aerosol emissions from GFED4s are lower than those from GFED3.1 in most of the savanna regions (e.g., SHAF, NHAF, and SHSA), even though the former includes smaller fires and has 11% higher global carbon emissions. This discrepancy between GFED4s and GFED3.1 can be partially explained by the fact that different emission factors were used to derive these two products, with the lower *EF* used for savanna in the former dataset taken from Andreae and Merlet (2001), whereas the higher *EF* used in the latter dataset was obtained from Akagi et al. (2011) (see Table 2). This situation will not change much even if the *EF* value from the latest estimation by Andreae (2019) were used, as explained earlier in Sect. 4.1.3.

Burning stages. Most current BB emission datasets do not distinguish the different burning stages, such as the flaming and smoldering stages that have distinctive emission characteristics. Typically, flaming dominates the earlier stage of the fire while smoldering dominates the later part. In the case of boreal forest fires, for example, about 40% of combustion originates from the flaming phase while 60% comes from the smoldering phase (Reid et al., 2005). In addition, smoldering combustion produces more OC and CO than flaming combustion; whereas flaming combustion produces more BC and carbon dioxide (CO_2) than smoldering (e.g., Freeborn et al., 2008).

4.3 Sources of the uncertainty associated with aerosol modeling

The model-related biases in the GEOS model, which other models most probably also suffer from, include, for example, inaccurate representations of horizontal and vertical transport of aerosol with wind, fire emission plume height, estimation of aerosol removal in models. Modeling of AOD properties such as optical properties and water uptake probably generates additional uncertainty. The ratio of OA to OC is 1.4 in this study, as first determined by White and Roberts (1977). However, this OA/OC ratio of 1.4 is at the low end of the generally suggested range of 1.2-2.5 (Turpin and Lim, 2001; Zhang et al., 2005; Bae et al., 2006; El-Zanan et al., 2006; Aiken et al., 2008; Chan et al., 2010). Observations suggest that OA/OC values of 1.6± 0.2 should be used for urban aerosols and 2.1± 0.2 for non-urban aerosols (Turpin and Lim, 2001). Enhancing this ratio can obviously increase the resulting AOD, but a more accurate measurement of this ratio during biomass burning is needed. Furthermore, the production of secondary organic aerosol (SOA) in biomass burning plumes, which has been observed in lab studies and ambient plumes (e.g., Bian et al., 2017; Ahern et al., 2019), are missing in these GEOS simulations. In addition, Ge et al. (2017) have shown that the choice of different meteorological fields, such as those from ECMWF and National Centers for Environmental Prediction (NCEP), can yield a factor of two difference in the resulting surface $PM_{2.5}$ concentration during the fire season of September in the Maritime continents.

5. Conclusions and recommendations

In this study, we compared six global biomass burning aerosol emission datasets in 2008, i.e., GFED3.1, GFED4s, FINN1.5, and GFAS1.2, FEER1.0 and QFED2.4. We also have examined the sensitivity of the modelled AOD to the different BB emission datasets in the NASA GEOS model globally and in 14-subregions. The main results are summarized as follows:

a. The biomass burning OC emissions derived from GFED3.1, GFED4s, FINN1.5, GFAS1.2, FEER1.0, and QFED2.4 can differ by up to a factor of 3.8 on an annual average, with values of 15.65, 13.76, 19.48, 18.22, 28.48, and 51.93 Tg C in 2008, respectively. The biomass burning BC emissions can differ by up to a factor of 3.4 on an annual average, with values of 1.76, 1.65, 1.83, 1.99, 3.66, and 5.54 Tg C in 2008, respectively. In general, higher biomass burning OC and BC emissions are estimated from QFED2.4 globally and regionally, followed by FEER1.0.
b. The best agreement among the six emission datasets occurred in Northern Hemisphere Africa (NHAF), Equatorial Asia (EQAS), Southern Hemisphere Africa (SHAF), and South Hemisphere South America (SHSA), where the biomass burning emissions are predominant in determining aerosol loading, with the top coefficient of variation ranks (1-4) and relatively low *max/min* ratio (a factor of 3-4). The least agreement occurred in the Middle East (MIDE), Temperate North America (TENA), Boreal North America (BONA), and Europe (EURO), with the bottom coefficient of variation ranks (14-11) and large *max/min* ratios (a factor of 66-10), as these are regions where biomass burning is either not dominant in total aerosol loading or QFED2.4 is extremely large. It seems that the diversity among the six BB emission datasets is largely driven by QFED2.4, which estimates the largest emission amount for almost all regions (except for equatorial Asia).
c. In Southern Hemisphere Africa (SHAF) and Southern Hemisphere South America (SHSA) during September 2008, where and when biomass burning aerosols are dominant over other aerosol types, the amounts of biomass burning OC emissions from QFED2.4 and FEER1.0 are at least double those from the remaining four BB emission datasets. The AOD simulated by the NASA GEOS based on these two BB emission datasets are the closest to those from MISR and AERONET, but still biased low. In particular, at Alta Floresta in SHSA, they can account for 36%-100% of the observed AOD, and at Mongu in SHAF, the AOD simulated with the six biomass burning emission datasets only account for 15%-49% of the observed AOD. Overall, during the biomass burning peak seasons at most of the representative AERONET sites selected in each region, the AOD simulated with QFED2.4 is the highest and closest to AERONET and MISR observations, followed by that of FEER1.0. Considering that regional scale transport and removal processes as well as wind fields are the same across the six BB emission experiments since they were run under the same model configurations except for BB emission, it is evident that enhancement of BB emission amounts in all six BB emission datasets except for QFED2.4 (although to different degrees) will be needed for the model AOD simulations to match observations, particularly in SHAF (Mongu) and SHSA (Alta Floresta). Although the result of this study is partially model-dependent, nevertheless, it sheds some light on our understanding of the uncertainty of the simulated AOD associated with the choice of biomass burning aerosol emission datasets.

Based on the results of the current study, it is appropriate to make some recommendations for future studies on improving BB emission estimation. Our understanding of the complexity, variability, and interrelationships between different fire characteristics (behavior, energetics, emissions) still need to be improved (Hyer et al, 2011). More accurate estimation of emission factors (*EF*) for different ecosystem types

and burning stages would greatly improve the emission overall, as demonstrated by the discrepancy between GFED3.1 and GFED4s (see Sect. 4.1.3). The global BB emission datasets driven by fire remote sensing and retrievals of FRP and burned-area products, which have hitherto depended heavily on MODIS, can be augmented with products from higher resolution sensors such as Visible Infrared Imaging Radiometer Suite (VIIRS), and the global suite of geostationary meteorological satellites such as Meteosat (covering Europe, Africa and the Indian Ocean), Geostationary Operational Environmental Satellite (GOES, covering North, Central, and South America) and Himawari (covering east Asia, southeast Asia, and Australia). Also, measurements from the recent field campaigns such as WE-CAN (https://www.eol.ucar.edu/field_projects/we-can) and FIREX-AQ (https://www.esrl.noaa.gov/csd/projects/firex-aq/science/motivation.html) are expected to contribute toward advancing our knowledge of biomass burning emissions in North America. The evaluation in this study has been solely based on remote sensing AOD data, including retrievals from both satellite (MIISR) and ground-based (AERONET) sensors. Continuous mass concentration measurements are needed to validate the fire-generated aerosol loading in specific contexts, such as in analyzing collocated surface and vertical aerosol concentrations and composition, at least in the major BB regions.

Data availability

The GFED3.1 biomass burning dataset can be accessed through the link: https://daac.ornl.gov/VEGETATION/guides/global_fire_emissions_v3.1.html. The link to the GFED4s dataset is http://www.globalfiredata.org. The FINN1.5 emissions dataset is archived at: http://bai.acom.ucar.edu/Data/fire/. The GFAS1.2 emissions dataset is downloaded at: https://apps.ecmwf.int/datasets/data/cams-gfas/. The FEER1.0 dataset is available at http://feer.gsfc.nasa.gov/data/emissions/. The QFED2.4 can be downloaded from the website : https://portal.nccs.nasa.gov/datashare/iesa/aerosol/emissions/QFED/v2.4r6/. MISR level 3 AOD data can be downloaded from website: https://eosweb.larc.nasa.gov/project/misr/mil3mae_table. AERONET Version 3 Level 2.0 data can be downloaded from the websites: https://aeronet.gsfc.nasa.gov/new_web/download_all_v3_aod.html. The GEOS model results can be provided by contacting with the corresponding author.

Author contribution

CI, MC, and XP conceived this project. XP conducted the data analysis and the model experiments. XP and CI wrote the majority of this manuscript, and all other authors participated in the writing process and interpretation of the results. HB, AD, PC and AS helped on model set-up. CI, AD, and LE provided the biomass burning emission datasets and interpretation of these datasets. TK, JW, and GC provided the help to apply the biomass burning emission datasets in the model. CI and MC provided funding supports.

Acknowledgement

MISR AOD data were obtained from the NASA Langley Research Center Atmospheric Science Data Center. We thank the AERONET networks for making their data available. Site PIs and data managers of those networks are gratefully acknowledged. We acknowledge the use of imagery from the NASA Worldview application (https://worldview.earthdata.nasa.gov), part of the NASA Earth Observing System Data and Information System (EOSDIS). Computing resources

supporting this work were provided by the NASA High-End Computing (HEC) Program through the NASA Center for Climate Simulation (NCCS) at Goddard Space Flight Center. We also thank the providers of biomass burning emission datasets of GFED, FINN, and GFAS. We acknowledge supports from various NASA earth science programs, including the NASA Atmospheric Composition Modeling, Analysis, and Prediction Program (ACMAP), the Modeling, Analysis, and Prediction program (MAP), the Interdisciplinary Studies Program (IDS), and Carbon Cycle Science program. CI is also grateful for partial support received during the preparation of this article from the Educational Partnership Program of the National Oceanic and Atmospheric Administration (NOAA), U.S. Department of Commerce, under Agreement No. #NA16SEC4810006. TO is supported by NASA under Grant No. NNX14AM76G. We appreciate the constructive comments from two reviewers, which help us to improve the quality of this manuscript. XP also acknowledges the valuable suggestions from Dr. Dongchul Kim. The contents of this article are solely the responsibility of the authors and do not represent the official views of any agency or institution.

Reference

Ahern, A. T., Robinson, E. S., Tkacik, D. S., Saleh, R., Hatch, L. E., Barsanti, K. C., et al. Production of secondary organic aerosol during aging of biomass burning smoke from fresh fuels and its relationship to VOC precursors. Journal of Geophysical Research: Atmospheres,124. https://doi.org/10.1029/2018JD029068, 2019.

Aiken, A. C., Decarlo, P. F., Kroll, J. H., Worsnop, D. R., Huffman, J. A., Docherty, K. S., Ulbrich, I. M., Mohr, C., Kimmel, J. R., Sueper, D., Sun, Y., Zhang, Q., Trimborn, A., Northway, M., Ziemann, P. J., Canagaratna, M. R., Onasch, T. B., Alfarra, M. R., Prevot, A. S. H., Dommen, J., Duplissy, J., Metzger, A., Baltensperger, U., and Jimenez, J. L.: O/C and OM/OC ratios of primary, secondary, and ambient organic aerosols with highresolution time-of-flight aerosol mass spectrometry, Environ. Sci. Technol., 42, 4478–4485, doi:10.1021/es703009q, 2008.

Akagi, S. K., Yokelson, R. J., Wiedinmyer, C., Alvarado, M. J., Reid, J. S., Karl, T., Crounse, J. D., and Wennberg, P. O.: Emission factors for open and domestic biomass burning for use in atmospheric models, Atmos. Chem. Phys., 11, 4039–4072, https://doi.org/10.5194/acp-11-4039-2011, 2011.

Andreae, M. O.: Emission of trace gases and aerosols from biomass burning – an updated assessment, Atmos. Chem. Phys., 19, 8523–8546, https://doi.org/10.5194/acp-19-8523-2019, 2019.

Andreae, M. O. and Merlet, P.: Emission of trace gases and aerosols from biomass burning, Global Biogeochem. Cy., 15, 955–966, https://doi.org/10.1029/2000GB001382, 2001.

Aurell, J., Mitchell B., Greenwell D., Holder A., Tabor D., Kiros F., and Gullett B.: Measuring Emission Factors from Open Fires and Detonations. AWMA Air Quality Measurement Methods and Technology, Durham, North Carolina, April 02 - 04, 2019.

Bae, M. S., Demerjian, K. L., and Schwab, J. J.: Seasonal estimation of organic mass to organic carbon in PM2.5at rural and urban locations in New York state, Atmos. Environ., 40, 7467–7479, 2006.

Bian, H., M. Chin, R. Kawa, B. Duncan, A. Arellano Jr., and R. Kasibhatla, Uncertainty of global CO simulations constraint by biomass burning emissions. J. Geophys. Res., 112, D23308, doi:10.1029/2006JD008376, 2007.

Bian, H., Chin, M., Rodriguez, J. M., Yu, H., Penner, J. E., and Strahan, S.: Sensitivity of aerosol optical thickness and aerosol direct radiative effect to relative humidity, Atmos. Chem. Phys., 9, 2375-2386, https://doi.org/10.5194/acp-9-2375-2009, 2009.

Bian, H., M. Chin, S. R. Kawa, H. Yu, T. Diehl, Multi-scale carbon monoxide and aerosol correlations from MOPITT and MODIS satellite measurements and GOCART model: implication for their emissions and atmospheric evolutions, J. Geophys. Res., 115, D07302, doi:10.1029/2009JD012781, 2010.

Bian, H., P. Colarco, M. Chin, G. Chen, J.M. Rodriguez, Q. Liang, et al. Investigation of source attributions of pollution to the Western Arctic during the NASA ARCTAS field campaign. Atmos. Chem. and Phys., 13, 4707-4721, doi:10.5194/acp-13-4707-2013, 2013.

Bian, Q., Jathar, S. H., Kodros, J. K., Barsanti, K. C., Hatch, L. E., May, A. A., Kreidenweis, S. M., and Pierce, J. R.: Secondary organic aerosol formation in biomass-burning plumes: theoretical analysis of lab studies and ambient plumes, Atmos. Chem. Phys., 17, 5459-5475, https://doi.org/10.5194/acp-17-5459-2017, 2017.

Bond, T., Doherty, S. J., Fahey, D. W., Forster, P. M., Berntsen, T., DeAngelo, B. J., Flanner, M. Ghan, Kärcher, B., Koch, D., Kinne, S., Kondo, Y., Quinn, P. Sarofim, M. C., Schultz, M., Schulz, M., Venkataraman, C., Zhang, H., Zhang, S., Bellouin, N. Guttikunda, S. Hopke, P. K., Jacobson, M. Z., Kaiser, J. W., Klimont, Z., Lohmann, U., Schwarz, J. P., Shindell, D., Storelvmo, T., Warren, S. G., and Zender, C. S.: Bounding the role of black carbon in the climate system: A scientific assessment, J. Geophys. Res., 118, 5380–5552, doi:10.1002/jgrd.50171, 2013.

Buchard, V., C. A. Randles, A. da Silva, A. S. Darmenov, et al.The MERRA-2 Aerosol Reanalysis,1980-onward, Part II: Evaluation and Case Studies. Journal of Climate, doi:10.1175/jclid-16-0613.1, 2017.

Burling, I. R., Yokelson, R. J., Akagi, S. K., Urbanski, S. P., Wold, C. E., Griffith, D. W. T., Johnson, T. J., Reardon, J., and Weise, D. R.: Airborne and ground-based measurements of the trace gases and particles emitted by prescribed fires in the United States, Atmos. Chem. Phys. Discuss., 11, 18677–18727, doi:10.5194/acpd-11-18677-2011, 2011.

Chan, T. W., Huang, L., Leaitch, W. R., Sharma, S., Brook, J. R., Slowik, J. G., Abbatt, J. P. D., Brickell, P. C., Liggio, J., Li, S.-M., and Moosmüller, H.: Observations of

OM/OC and specific attenuation coefficients (SAC) in ambient fine PM at a rural site in central Ontario, Canada, Atmos. Chem. Phys., 10, 2393-2411, https://doi.org/10.5194/acp-10-2393-2010, 2010.

Chin, M., R. B. Rood, S.-J. Lin, J.-F. Müller, and A. M. Thompson, Atmospheric sulfur cycle in the global mdel GOCART: Model description and global properties, J. Geophys. Res., 105, 24,661-24,687, 2000.

Chin, M., P. Ginoux, S. Kinne, O. Torres, B. N. Holben, B. N. Duncan, R. V. Martin, J. A. Logan, A. Higurashi, and T. Nakajima, Tropospheric aerosol optical thickness from the GOCART model and comparisons with satellite and sun photometer measurements, J. Atmos., Sci., 59, 461-483, 2002.

Chin, M., T. Diehl, O. Dubovik, T. F. Eck, B. N. Holben, A. Sinyuk, and D. G. Streets, Light absorption by pollution, dust and biomass burning aerosols: A global model study and evaluation with AERONET data, Ann. Geophys., 27, 3439-3464, 2009.

Chin, M., T. Diehl, Q. Tan, J. M. Prospero, R. A. Kahn, L. A. Remer, H. Yu, A. M. Sayer, H. Bian, I. V. Geogdzhayev, B. N. Holben, S. G. Howell, B. J. Huebert, N. C. Hsu, D. Kim, T. L. Kucsera, R. C. Levy, M. I. Mishchenko, X. Pan, P. K. Quinn, G. L. Schuster, D. G. Streets, S. A. Strode, O. Torres, and X.-P. Zhao, Multi-decadal variations of atmospheric aerosols from 1980 to 2009: a perspective from observations and a global model, Atmos. Chem. Phys., 14, 3657-3690, 2014.

Chou, M.-D. and M. J. Suarez, A solar radiation parameterization for atmospheric studies, NASA/TM-1999- 104606, Vol. 15, 1999.

Chou, M.-D., M. J. Suarez, X.-Z. Liang, and M.-H. Yan, A thermal infrared radiation parameterization for atmospheric studies. NASA Tech. Memo. 104 606, 55 pp, 2001.

Christian, T., Kleiss, B., Yokelson, R. J., Holzinger, R., Crutzen, P. J., Hao, W. M., Saharjo, B. H., and Ward, D. E.: Comprehensive laboratory measurements of biomass-burning emissions: 1. Emissions from Indonesian, African, and other fuels, J. Geophys. Res., 108(D23), 4719, doi:10.1029/2003JD003704, 2003.

Colarco, P. R., A. da Silva, M. Chin, T. Diehl. Online simulations of global aerosol distributions in the NASA GEOS-4 model and comparisons to satellite and ground-based aerosol optical depth, J. Geophys. Res., 115, D14207, doi:10.1029/2009JD012820, 2010.

Darmenov, A. and da Silva. A. The quick fire emissions dataset (QFED)–documentation of versions 2.1, 2.2 and 2.4, NASA Technical Report Series on Global Modeling and Data Assimilation, NASA TM-2015-104606, 38, 2015.

Eck, T. F., Holben, B. N., Ward, D. E., Dubovik, O., Reid, J. S., Smirnov, A., et al.. Characterization of the optical properties of biomass burning aerosols in Zambia during

the 1997 ZIBBEE field campaign. Journal of Geophysical Research, 106(D4), 3425–3448. https://doi.org/10.1029/2000JD900555, 2001.

El-Zanan, H. S., Lowenthal, D. H., Zielinska, B., Chow, J. C., and Kumar, N.: Determination of the organic aerosol mass to organic carbon ratio in IMPROVE samples, Chemosphere, 60, 485–496, 2005.

Freeborn, P. H., M. J. Wooster, W. M. Hao, C. A. Ryan, B. L. Nordgren, S. P. Baker, and C. Ichoku. Relationships between energy release, fuel mass loss, and trace gas and aerosol emissions during laboratory biomass fires, J. Geophys. Res., 113, D01301, doi:10.1029/2007JD008679, 2008.

Ge, C., J. Wang, J. S. Reid, D. Posselt, P. Lynch, E. Hyer, Mesoscale modeling of smoke transport from equatorial Southeast Asian Maritime Continent to the Philippines: First comparison of ensemble analysis with in situ observations, *J. Geophys. Res.- Atmos.*, 122, 5380–5398, 2017.

Gelaro, R., W. McCarty, M.J. Suárez, R. Todling, A. Molod, L. Takacs, C.A. Randles, A. Darmenov, M.G. Bosilovich, R. Reichle, K. Wargan, L. Coy, R. Cullather, C. Draper, S. Akella, V. Buchard, A. Conaty, A.M. da Silva, W. Gu, G. Kim, R. Koster, R. Lucchesi, D. Merkova, J.E. Nielsen, G. Partyka, S. Pawson, W. Putman, M. Rienecker, S.D. Schubert, M. Sienkiewicz, and B. Zhao: The Modern-Era Retrospective Analysis for Research and Applications, Version 2 (MERRA-2). J. Climate, 30, 5419–5454, https://doi.org/10.1175/JCLI-D-16-0758.1, 2017.

Giglio, L., Randerson, J. T., van der Werf, G. R., Kasibhatla, P. S., Collatz, G. J., Morton, D. C., and DeFries, R. S.: Assessing variability and long-term trends in burned area by merging multiple satellite fire products, Biogeosciences, 7, 1171–1186, https://doi.org/10.5194/bg-7-1171-2010, 2010.

Giglio, L., Randerson, J. T., and van der Werf, G. R.: Analysis of daily, monthly, and annual burned area using the fourth-generation global fire emissions database (GFED4), J. Geophys.Res.-Biogeo., 118, 317–328, https://doi.org/10.1002/jgrg.20042, 2013.

Giles, D. M., Sinyuk, A., Sorokin, M. G., Schafer, J. S., Smirnov, A., Slutsker, I., Eck, T. F., Holben, B. N., Lewis, J. R., Campbell, J. R., Welton, E. J., Korkin, S. V., and Lyapustin, A. I.: Advancements in the Aerosol Robotic Network (AERONET) Version 3 database – automated near-real-time quality control algorithm with improved cloud screening for Sun photometer aerosol optical depth (AOD) measurements, Atmos. Meas. Tech., 12, 169-209,https://doi.org/10.5194/amt-12-169-2019, 2019.

Hawbaker, T. J., Radeloff, V. C., Syphard, A. D., Zhu, Z. L., and Steward, S. I.: Detection rates of the MODIS active fire product in the United States. Remote Sens. Environ., 112(5) 2656–2664, 2008.

1118 Hoelzemann, J. J., Schultz, M. G., Brasseur, G. P., Granier, C., and Simon, M.: Global
1119 Wildland Fire Emission Model (GWEM): Evaluating the use of global area burnt satellite
1120 data, J. Geophys. Res., 109, D14S04, doi:10.1029/2003JD003666, 2004.
1121
1122 Holben, B. N., Eck, T. F., Slutsker, I., Tanre, D., Buis, J. P., Setzer, A., Vermote, E.,
1123 Reagan, J. A., Kaufman, Y. J., Nakajima, T., Lavenu, F., Jankowiak, I., and Smirnov, A.:
1124 AERONET – a federated instrument network and data archive for aerosol
1125 characterization, Remote Sens. Environ. 66, 1–16, 1998.
1126
1127 Hyer, E. J., and J. S. Reid. Baseline uncertainties in biomass burning emission models
1128 resulting from spatial error in satellite active fire location data, Geophys. Res. Lett., 36,
1129 L05802, doi:10.1029/2008GL036767, 2009.
1130
1131 Hyer, E. J., J. S. Reid, and J. Zhang: An over-land aerosol optical depth data set for data
1132 assimilation by filtering, correction, and aggregation of MODIS collection 5 optical depth
1133 retrievals, Atmos. Meas. Tech., 4, 379–408, doi:10.5194/amt-4-379-2011, 2011.
1134
1135 Ichoku, C., and Ellison, L.Global top-down smoke-aerosol emissions estimation using
1136 satellite fire radiative power measurements. Atmospheric Chemistry and Physics, 14(13),
1137 6643-6667. doi:10.5194/acp-14-6643-2014, 2014.
1138
1139 Ichoku, C., Ellison, L. T., Yue, Y., Wang, J., & Kaiser, J. W. Fire and Smoke Remote
1140 Sensing and Modeling Uncertainties. Natural Hazard Uncertainty Assessment: Modeling
1141 and Decision Support, 215-230, doi: 10.1002/9781119028116.ch14, 2016a.
1142
1143 Ichoku, C., Ellison, L.T., Willmot, K.E., Matsui, T., Dezfuli, A.K., Gatebe, C.K., Wang,
1144 J., Wilcox, E.M., Lee, J., Adegoke, J. and Okonkwo, C. Biomass burning, land-cover
1145 change, and the hydrological cycle in Northern sub-Saharan Africa. *Environmental
1146 Research Letters*, *11*(9), p.095005, 2016b.
1147
1148 Ichoku, C., L. Giglio, M. J. Wooster, and L. A. Remer. Global characterization of
1149 biomass-burning patterns using satellite measurements of fire radiative energy. Remote
1150 Sensing of Environment, 112 (6): 2950-2962 [10.1016/j.rse.2008.02.009], 2008.
1151
1152 Ichoku, C., R. Kahn, and M. Chin. Satellite contributions to the quantitative
1153 characterization of biomass burning for climate modeling, Atmos. Res., 111, 1–28, 2012.
1154
1155 Ichoku, C., and Y. Kaufman. A method to derive smoke emission rates from MODIS fire
1156 radiative energy measurements.*IEEE Trans on Geosc & Rem Sens*, **43 (11):** 2636-2649
1157 [10.1109/TGRS.2005.857328], 2005.
1158
1159 Janssens-Maenhout, G., Crippa, M., Guizzardi, D., Dentener, F., Muntean, M., Pouliot,
1160 G., Keating, T., Zhang, Q., Kurokawa, J., Wankmüller, R., Denier van der Gon, H.,
1161 Kuenen, J. J. P., Klimont, Z., Frost, G., Darras, S., Koffi, B., and Li, M.: HTAP_v2.2: a
1162 mosaic of regional and global emission grid maps for 2008 and 2010 to study

hemispheric transport of air pollution, Atmos. Chem. Phys., 15, 11411–11432, https://doi.org/10.5194/acp-15-11411-2015, 2015.

Jordan, N., Ichoku, C., and Hoff, R.: Estimating smoke emissions over the U.S. Southern Great Plains using MODIS fire radiative power and aerosol observations, Atmos. Env., 42, 2007–2022, 2008.

Kahn, R.A., Gaitley B.J., Garay M.J., Diner D.J., Eck T., Smirnov A., and Holben B.N.: Multiangle Imaging SpectroRadiometer global aerosol product assessment by comparison with the Aerosol Robotic Network. *J. Geophys. Res*. 115, D23209, doi: 10.1029/2010JD014601, 2010.

Kalashnikova O. V., and Kahn R.A.: Ability of multiangle remote sensing observations to identify and distinguish mineral dust types: Part 2. Sensitivity over dark water *J. Geophys. Res*., D11207, 111 10.1029/2005JD006756, 2006.

Kaiser, J. W., Heil, A., Andreae, M. O., Benedetti, A., Chubarova, N., Jones, L., Morcrette, J.-J., Razinger, M., Schultz, M. G., Suttie, M., and van der Werf, G. R.: Biomass burning emissions estimated with a global fire assimilation system based on observations of fire radiative power, Biogeosciences, 9, 527-554, doi:10.5194/bg-9-527-2012, 2012.

Kaiser, J.W., Flemming, J., Schultz, M. G., Suttie, M., andWooster, M. J.: The MACC Global Fire Assimilation System: First Emission Products (GFASv0), Tech. Memo. 596, ECMWF, Reading,UK, 2009.

Kaufman, Y. J., C. O. Justice, L. P. Flynn, J. D. Kendall, E. M. Prins, L. Giglio, D. E. Ward, W. P. Menzel, and A. W. Setzer. Potential global fire monitoring from EOS-MODIS, J. Geophys. Res., 103(D24), 32,215–32,238, doi:10.1029/98JD01644, 1998.

Liousse, B., Guillaume, J. M., Grégoire, M., Mallet, C., Galy, C., Pont, V., Akpo, A., Bedou, M., Castéra, P., Dungall, L., Gardrat, E., Granier, C., Konaré, A., Malavelle, F., Mariscal, A., Mieville, A., Rosset, R., Serça, D., Solmon, F., Tummon, F., Assamoi, E., Yoboué, V., and Van Velthoven, P.: Updated African biomass burning emission inventories in the framework of the AMMAIDAF program, with an evaluation of combustion aerosols, Atmos. Chem. Phys., 10, 7347–7382, doi:10.5194/acp-10-7347-2010, 2010.

Molod, A. M., L. L. Takacs, M. J. Suarez, and J. Bacmeister. Development of the GEOS atmospheric general circulation model: evolution from MERRA to MERRA2 ." Geosci. Model Dev. 8 1339-1356 [10.5194/gmd-8-1339-2015], 2015.

Pan, X., Chin, M., Gautam, R., Bian, H., Kim, D., Colarco, P. R., Diehl, T. L., Takemura, T., Pozzoli, L., Tsigaridis, K., Bauer, S., and Bellouin, N.: A multi-model evaluation of aerosols over South Asia: common problems and possible causes, Atmos. Chem. Phys., 15, 5903-5928, https://doi.org/10.5194/acp-15-5903-2015, 2015.

Pan, X., Chin, M., Ichoku, C. M., & Field, R. D. Connecting Indonesian fires and drought with the type of El Niño and phase of the Indian Ocean dipole during 1979–2016. Journal of Geophysical Research: Atmospheres, 123. https://doi.org/10.1029/2018JD028402, 2018.

Peterson, D., & Wang, J. A Sub-pixel-based calculate of fire radiative power from MODIS observations: 2. Sensitivity analysis and potential fire weather application. Remote Sensing of Environment, 129, 231–249, 2013.

Peterson, D. A., J. R. Campbell, E. J. Hyer, M. D. Fromm, G. P. Kablick, J. H. Cossuth, and M. T. DeLand. Wildfire-driven thunderstorms cause a volcano-like stratospheric injection of smoke. *npj Climate and Atmospheric Science*, **1,** 30, 2018.

Petrenko, M., R. Kahn, M. Chin, A. Soja, T. Kucsera, and Harshvardhan. The use of satellite-measured aerosol optical depth to constrain biomass burning emissions source strength in the global model GOCART, J. Geophys. Res., 117, D18212, doi:10.1029/2012JD017870, 2012.

Petrenko, M., Kahn, R., Chin, M., & Limbacher, J. Refined use of satellite aerosol optical depth snapshots to constrain biomass burning emissions in the GOCART model. Journal of Geophysical Research: Atmospheres, 122, 10,983–11,004. https://doi.org/10.1002/ 2017JD026693, 2017.

Pereira, G., Siqueira, R., Rosário, N. E., Longo, K. L., Freitas, S. R., Cardozo, F. S., Kaiser, J. W., and Wooster, M. J.: Assessment of fire emission inventories during the South American Biomass Burning Analysis (SAMBBA) experiment, Atmos. Chem. Phys.,16, 6961–6975, doi:10.5194/acp-16-6961-2016, 2016.

Randerson, J. T., Chen, Y., van der Werf, G. R., Rogers, B. M., and Morton, D. C.: Global burned area and biomass burning emissions from small fires, J. Geophys. Res.-Biogeo., 117, G04012, https://doi.org/10.1029/2012JG002128, 2012.

Randles, C. A., A. da Silva, V. Buchard, et al. 2017: The MERRA-2 Aerosol Reanalysis, 1980-onward, Part I: System Description and Data Assimilation Evaluation. J Clim, doi: 10.1175/jclid-16-0609.1

Reddington, C. L., Spracklen, D. V., Artaxo, P., Ridley, D. A., Rizzo, L. V., and Arana, A.: Analysis of particulate emissions from tropical biomass burning using a global aerosol model and long-term surface observations, Atmos. Chem. Phys., 16, 11083-11106, https://doi.org/10.5194/acp-16-11083-2016, 2016.

Reid, J. S., R. Koppmann, T. F. Eck, and D. P. Eleuterio. A review of biomass burning emissions part II: Intensive physical properties of biomass burning particles, Atmos. Chem. Phys., 5, 799–825, 2005.

Reid, C.E.; Brauer, M.; Johnston, F.H.; Jerrett, M.; Balmes, J.R.; Elliott, C.T. Critical Review of Health Impacts of Wildfire Smoke Exposure. Environ. Health Perspect, 124, 1334–1343, 2016.

Rienecker, M. M., M. J. Suarez, R. Gelaro, R. Todling, J. Bacmeister, E. Liu, M. G. Bosilovich, S. D. Schubert, L. Takacs, G.-K. Kim, S. Bloom, J. Chen, D. Collins, A. Conaty, A. da Silva, W. Gu, J. Joiner, R. D. Koster, R. Lucchesi, A. Molod, T. Owens, S. Pawson, P. Pegion, C. R. Redder, R. Reichle, F. R. Robertson, A. G. Ruddick, M. Sienkiewicz, J. Woollen, MERRA - NASA's Modern-Era Retrospective Analysis for Research and Applications. J. Climate, 24, 3624–3648, 2011.

Roberts, G., Wooster, M., & Lagoudakis, E. Annual and diurnal African biomass burning temporal dynamics. Biogeosciences, 6, 2009.

Saide, P. E., et al.: Revealing important nocturnal and day-to-day variations in fire smoke emissions through a multiplatform inversion, Geophys. Res. Lett.,42, 3609–3618,doi:10.1002/2015GL063737, 2015.

Simon, H. and Bhave, P. V.: Simulating the Degree of Oxidation in Atmospheric Organic Particles, Environ. Sci. Technol., 46, 331–339, doi:10.1021/es202361w, 2012.

Tansey, K., J. Beston, A. Hoscilo, S. E. Page, and C. U. Paredes Hernandez, Relationship between MODIS fire hotspot count and burned area in a degraded tropical peat swamp forest in Central Kalimantan, Indonesia,J. Geophys. Res.,113, D23112, doi:10.1029/2008JD010717, 2008.

Turpin, B. J. and Lim, H. J.: Species contributions to PM2.5 mass concentrations: Revisiting common assumptions for estimating organic mass, Aerosol Sci. Tech., 35, 602–610, doi:10.1080/02786820152051454, 2001.

van der Werf, G. R., Randerson, J. T., Giglio, L., Collatz, G. J., Kasibhatla, P. S., and Arellano Jr., A. F.: Interannual variability in global biomass burning emissions from 1997 to 2004, Atmos. Chem. Phys., 6, 3423–3441, https://doi.org/10.5194/acp-6-3423-2006, 2006.

van der Werf, G. R., Randerson, J. T., Giglio, L., Collatz, G. J., Mu, M., Kasibhatla, P. S., Morton, D. C., DeFries, R. S., Jin, Y., and van Leeuwen, T. T.: Global fire emissions and the contribution of deforestation, savanna, forest, agricultural, and peat fires (1997–2009), Atmos. Chem. Phys., 10, 11707–11735, https://doi.org/10.5194/acp-10-11707-2010, 2010.

van der Werf, G. R., Randerson, J. T., Giglio, L., van Leeuwen, T. T., Chen, Y., Rogers, B. M., Mu, M., van Marle, M. J. E., Morton, D. C., Collatz, G. J., Yokelson, R. J., and Kasibhatla, P. S.: Global fire emissions estimates during 1997–2016, Earth Syst. Sci. Data, 9, 697-720, https://doi.org/10.5194/essd-9-697-2017, 2017.

van Leeuwen, T. T., van der Werf, G. R., Hoffmann, A. A., Detmers, R. G., Ruecker, G., French, N. H. F., Archibald, S., Carvalho, J. A. J., Cook, G. D., de Groot, W. J., Hely, C., Kasischke, E. S., Kloster, S., McCarty, J. L., Pettinari, M. L., Savadogo, P., Alvarado, E. C., Boschetti, L., Manuri, S., Meyer, C. P., Siegert, F., Trollope, L. A. and Trollope, W. S. W.: Biomass burning fuel consumption rates: a field measurement database, Biogeosciences, 11(24), 7305–7329, doi:10.5194/bg-11-7305-2014, 2014.

van Marle, M. J. E., Kloster, S., Magi, B. I., Marlon, J. R., Daniau, A.-L., Field, R. D., Arneth, A., Forrest, M., Hantson, S., Kehrwald, N. M., Knorr, W., Lasslop, G., Li, F., Mangeon, S., Yue, C., Kaiser, J. W., and van der Werf, G. R.: Historic global biomass burning emissions for CMIP6 (BB4CMIP) based on merging satellite observations with proxies and fire models (1750–2015), Geosci. Model Dev., 10, 3329-3357, https://doi.org/10.5194/gmd-10-3329-2017, 2017.

Wang, J., C. Ge, Z. Yang, E. J. Hyer, J. S. Reid, B.-N. Chew, M. Mahmud, Y. Zhang, and M. Zhang, Mesoscale modeling of smoke transport over the Southeast Asian Maritime Continent: interplay of sea breeze, trade wind, typhoon, and topography, Atmospheric Research, 122, 486-503, doi: 10.1016/j.atmosres.2012.05.009, 2013.

Wang, J., S.A. Christopher, U.S. Nair, J.S. Reid, E.M. Prins, J. Szykman, and J.L. Hand, Mesoscale modeling of Central American smoke transport to the United States, 1: "top-down" assessment of emission strength and diurnal variation impacts, J. Geophys. Res., 11, D05S17, doi:10.1029/2005JD006416, 2006.

Wang, J., Yue, Y., Wang, Y., Ichoku, C., Ellison, L., & Zeng, J. Mitigating satellite-based fire sampling limitations in deriving biomass burning emission rates: Application to WRF-Chem model over the Northern sub-Saharan African Region. Journal of Geophysical Research: Atmospheres, 123, 507–528. https://doi.org/10.1002/2017JD026840, 2018.

White, W. H. and Roberts, P. T.: On the nature and origins of visibility-reducing aerosols in the Los Angeles air basin, Atmos. Environ., 11, 803–812, 1977.

Wiedinmyer, C., Akagi, S. K., Yokelson, R. J., Emmons, L. K., Al-Saadi, J. A., Orlando, J. J., and Soja, A. J. The Fire Inventory from NCAR (FINN): a high resolution global model to estimate the emissions from open burning, Geosci. Model Dev., 4, 625–641, doi:10.5194/gmd-4-625-2011, 2011.

Wooster, M. J., G. Roberts, G. L. W. Perry, and Y. J. Kaufman. Retrieval of biomass combustion rates and totals from fire radiative power observations: FRP derivation and calibration relationships between biomass consumption and fire radiative energy release, J. Geophys. Res., 110, D24311, doi:10.1029/2005JD006318, 2005.

Wooster, M. J., B. Zhukov, and D. Oertel. Fire radiative energy for quantitative study of biomass burning: Derivation from the BIRD experimental satellite and comparison to MODIS fire products, Remote Sens. Environ., 86(1), 83–107, doi:10.1016/S0034-4257(03)00070-1, 2003.

Yang, Z., J. Wang, C. Ichoku, E. Hyer, and J. Zeng, Mesoscale modeling and satellite observation of transport and mixing of smoke and dust particles over northern sub-Saharan African region, J. Geophys. Res. Atmos., 118, 12,139-12,157, doi:10.1002/2013JD020644, 2013.

Yokelson, R. J., Burling, I. R., Urbanski, S. P., Atlas, E. L., Adachi, K., Buseck, P. R., Wiedinmyer, C., Akagi, S. K., Toohey, D. W., and Wold, C. E.: Trace gas and particle emissions from open biomass burning in Mexico, Atmos. Chem. Phys., 11, 6787–6808, doi:10.5194/acp-11-6787-2011, 2011.

Zhang, F., J. Wang, C. M. Ichoku, et al.. Sensitivity of mesoscale modeling of smoke direct radiative effect to the emission inventory: a case study in northern sub-Saharan African region. Environmental Research Letters, 9 (7): 075002 (14 pp) [10.1088/1748-9326/9/7/075002], 2014.

Zhang, Q., Worsnop, D. R., Canagaratna, M. R., and Jimenez, J. L.: Hydrocarbon-like and oxygenated organic aerosols in Pittsburgh: insights into sources and processes of organic aerosols, Atmos. Chem. Phys., 5, 3289–3311, 2005b, http://www.atmos-chem-phys.net/5/3289/2005/.

Zhu, J., X. Xia, J. Wang, C. Wiedinmyer, J. A. Fisher, C. A. Keller. Impact of Southeast Asian smoke on aerosol properties in Southwest China: first comparison of model simulations with satellite and ground observation, J. Geophys. Res.-Atmos., 122, 3904–3919, 2017.

FIGURES

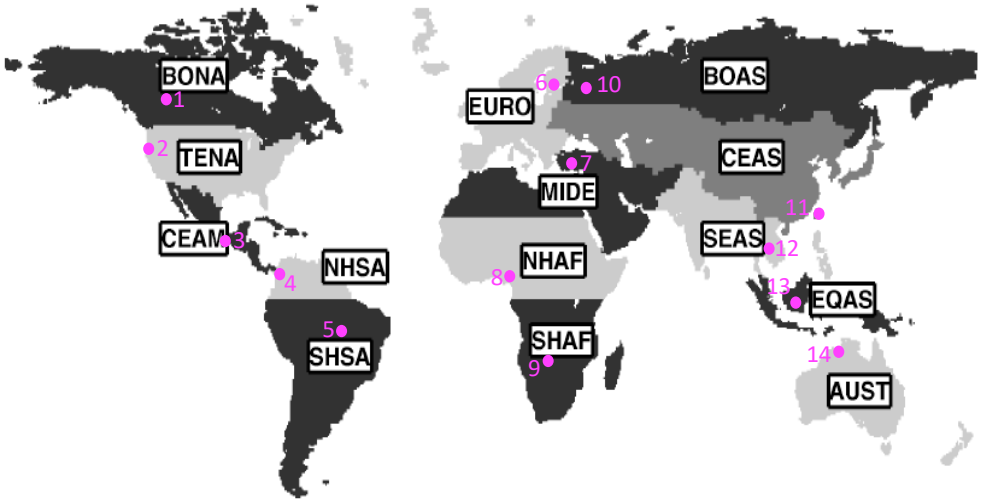

BONA	Boreal North America	NHAF	Northern Hemisphere Africa
TENA	Temperate North America	SHAF	Southern Hemisphere Africa
CEAM	Central America	BOAS	Boreal Asia
NHSA	Northern Hemisphere South America	CEAS	Central Asia
SHSA	Southern Hemisphere South America	SEAS	Southeast Asia
EURO	Europe	EQAS	Equatorial Asia
MIDE	Middle East	AUST	Australia and New Zealand

Figure 1. Map showing the 14 regions used in this study, following GFED regionalization defined by Giglio et al. (2006) and van der Werf et al. (2006; 2017). The fourteen AERONET sites selected for detailed analysis in the respective regions are represented by the numbered magenta dots. These AERONET sites and the included data years (in parentheses) for calculating aerosol climatology are: 1-Fort McMurray (2005-2018), 2-Monterey (2002-2018), 3-Tuxtla Gutierrez (2005-2010), 4-Medellin (2012-2016), 5-Alta Floresta (1993-2018), 6-Toravere (2002-2017), 7-IMS METU ERDEMLI (1999-2017), 8-Ilorin (1998-2018), 9-Mongu (1997-2010), 10-Moscow MSU MO (2001-2017), 11-EPA NCU (2004-2018), 12-Chiang Mai Met Sta (2007-2017), 13-Palangkaraya (2012-2017), 14-Lake Argyle (2001-2017).

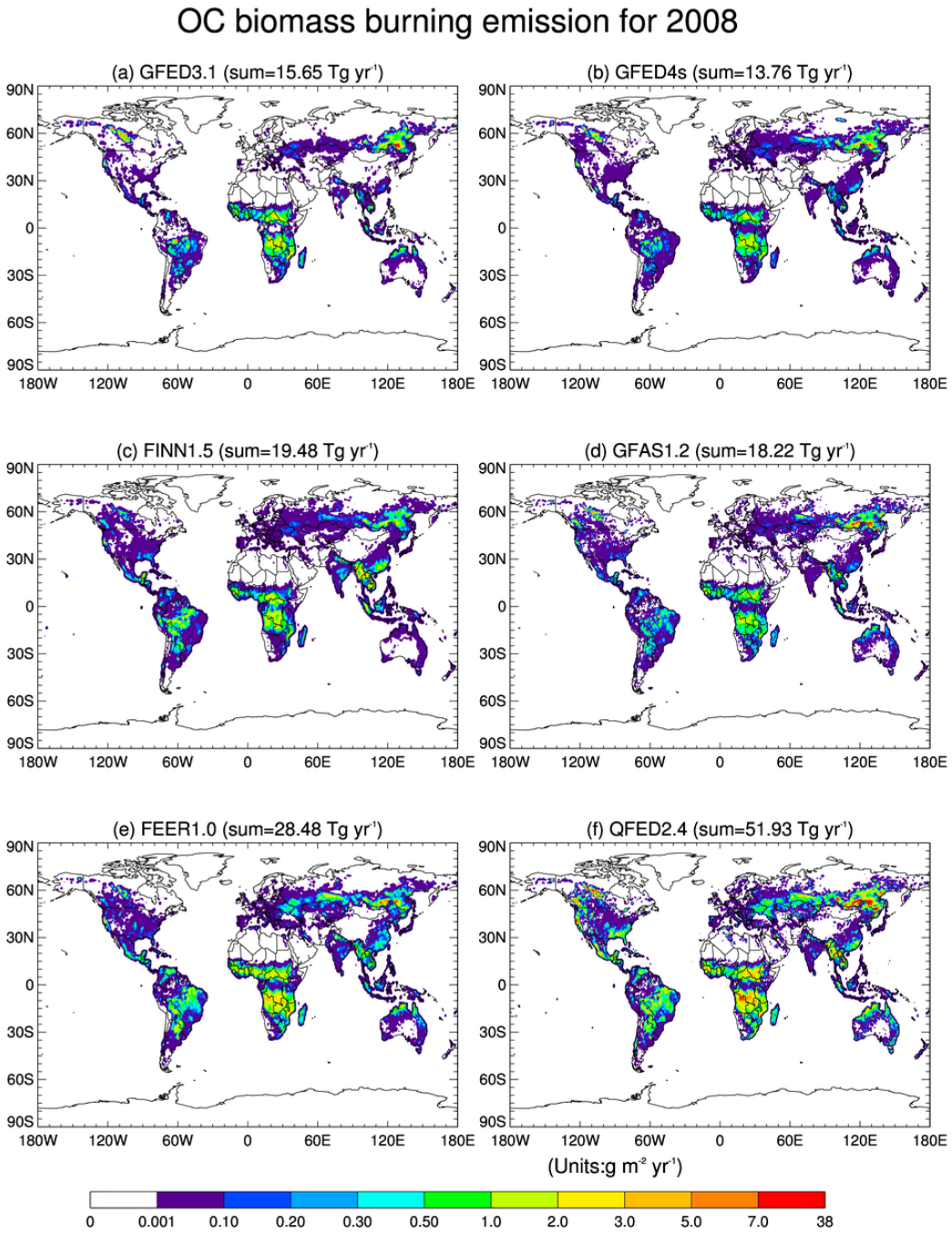

Figure 2. The spatial distribution of annual total organic carbon biomass burning emissions for 2008 estimated by six biomass burning emission datasets (units: g m^{-2} yr^{-1}). The global total amount is indicated in the parentheses.

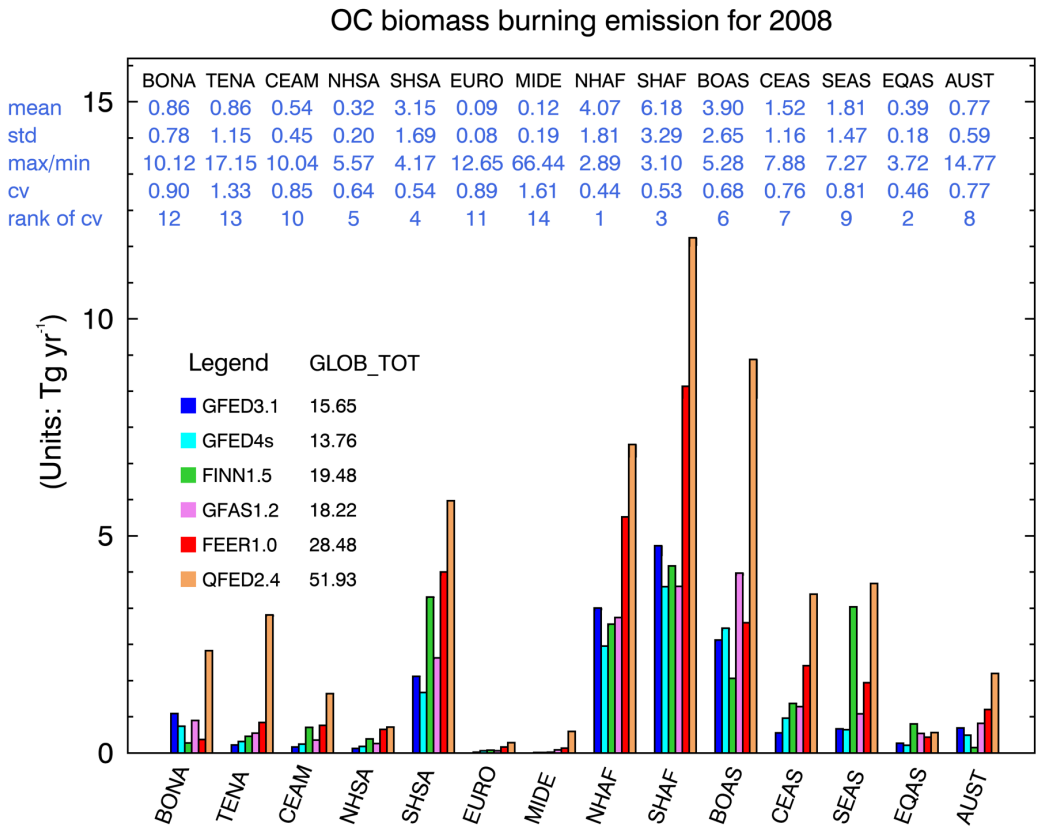

Figure 3. The regional annual total organic carbon biomass burning emissions for 2008 in six biomass burning emission datasets in 14 regions (units: Tg yr^{-1}). The global annual total amount is listed after the name of each dataset (GLOB_TOT). Relevant statistics for the six BB emission datasets in each region are also listed under the short name of each region on the top of the panel in blue, with the mean of the six BB emission datasets in the first row. Three different methods to measure the spread of the six BB emission datasets are shown as well: one absolute method, i.e., the standard deviation (std) in the second row, and two relative methods, i.e., the ratio of max to min (i.e., maximum/minimum) shown in the third row, and the coefficient of variation (cv), defined as the ratio of the std to the mean, in the fourth row. The rankings of the regions regarding the spread of the BB emissions datasets according to cv are shown in the fifth row (i.e., a ranking of 1 means that this region shows the least spread among the six BB emissions datasets, while a ranking of 14 indicates that this region has the largest spread among the 14 regions).

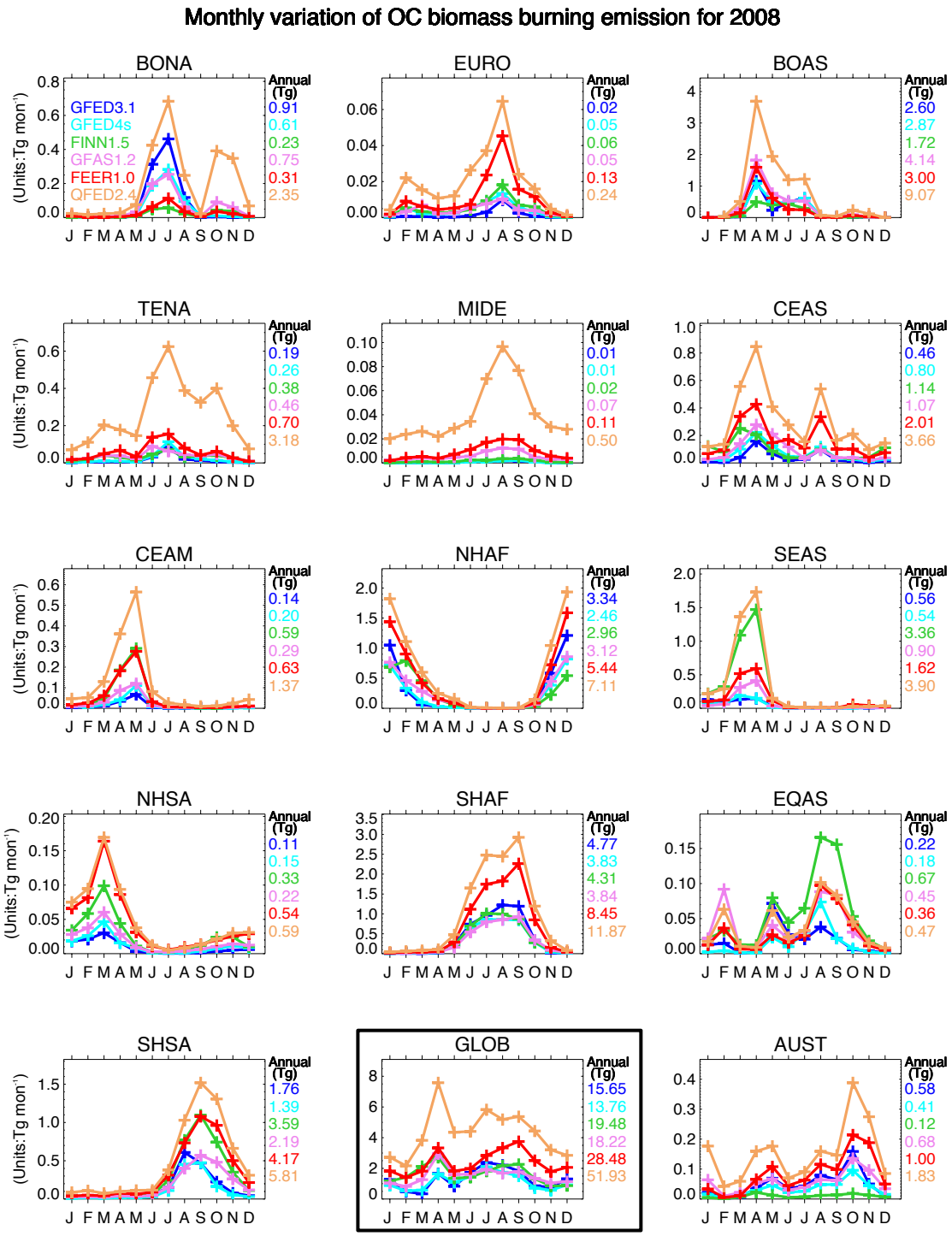

Figure 4. Monthly variation of organic carbon biomass burning emissions for 2008 in six biomass burning emission datasets in 14 regions and the globally (i.e., GLOB, highlighted with a black box). The annual total emission is listed on the right side of each panel.

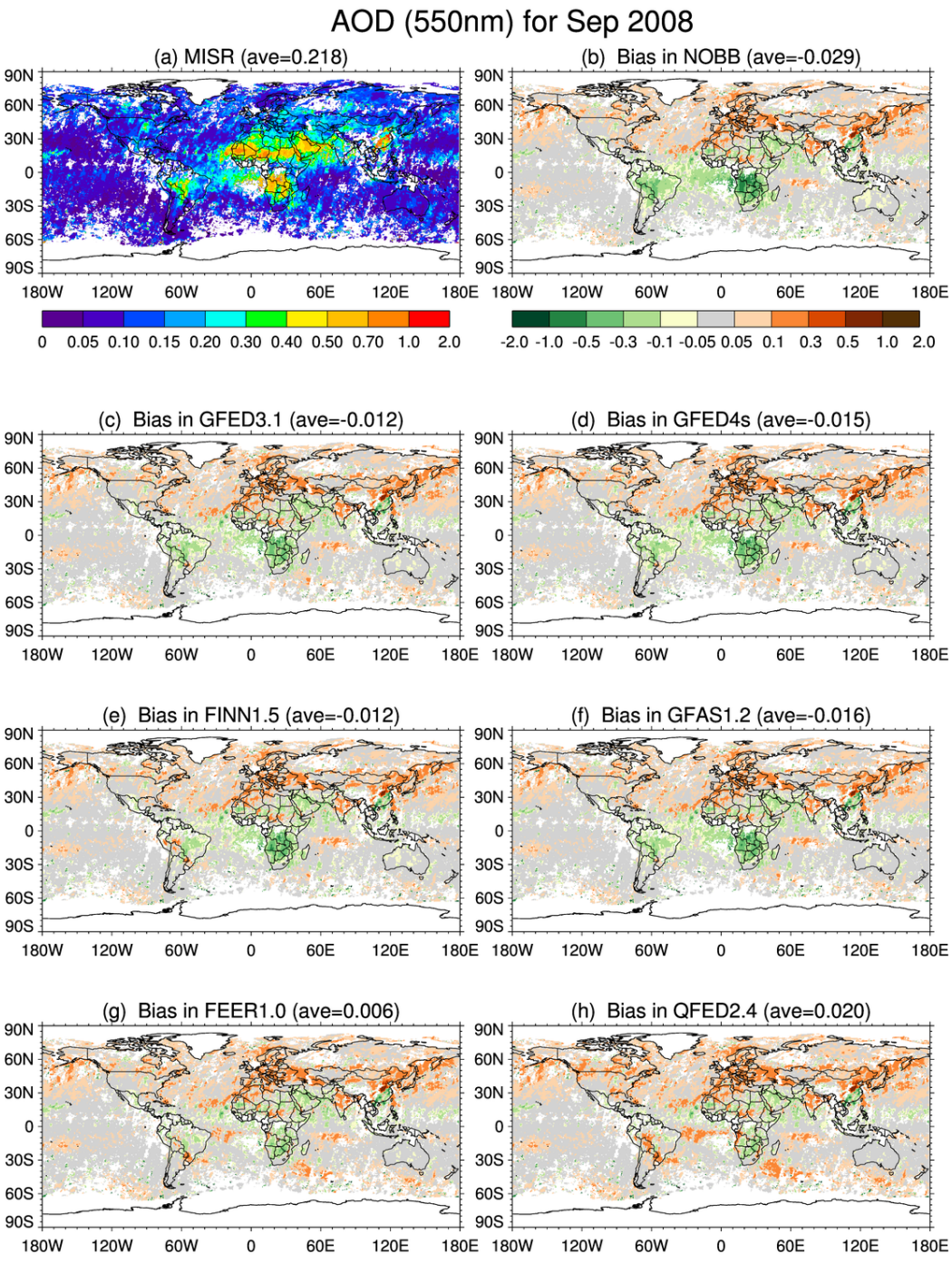

Figure 5. (a) The spatial distribution of monthly mean AOD at 558nm for September 2008 from MISR with the white color representing missing value. The global averaged value (ave) is shown in the parentheses. (b)-(h) are for GEOS model biases (i.e., model at 550nm minus MISR at 558nm) in seven model experiments, i.e., bias in (b) NOBB, (c) GFED3.1, (d) GFED4s, (e) FINN1.5, (f) GFAS1.2, (g) FEER1.0, (h) QFED2.4, respectively.

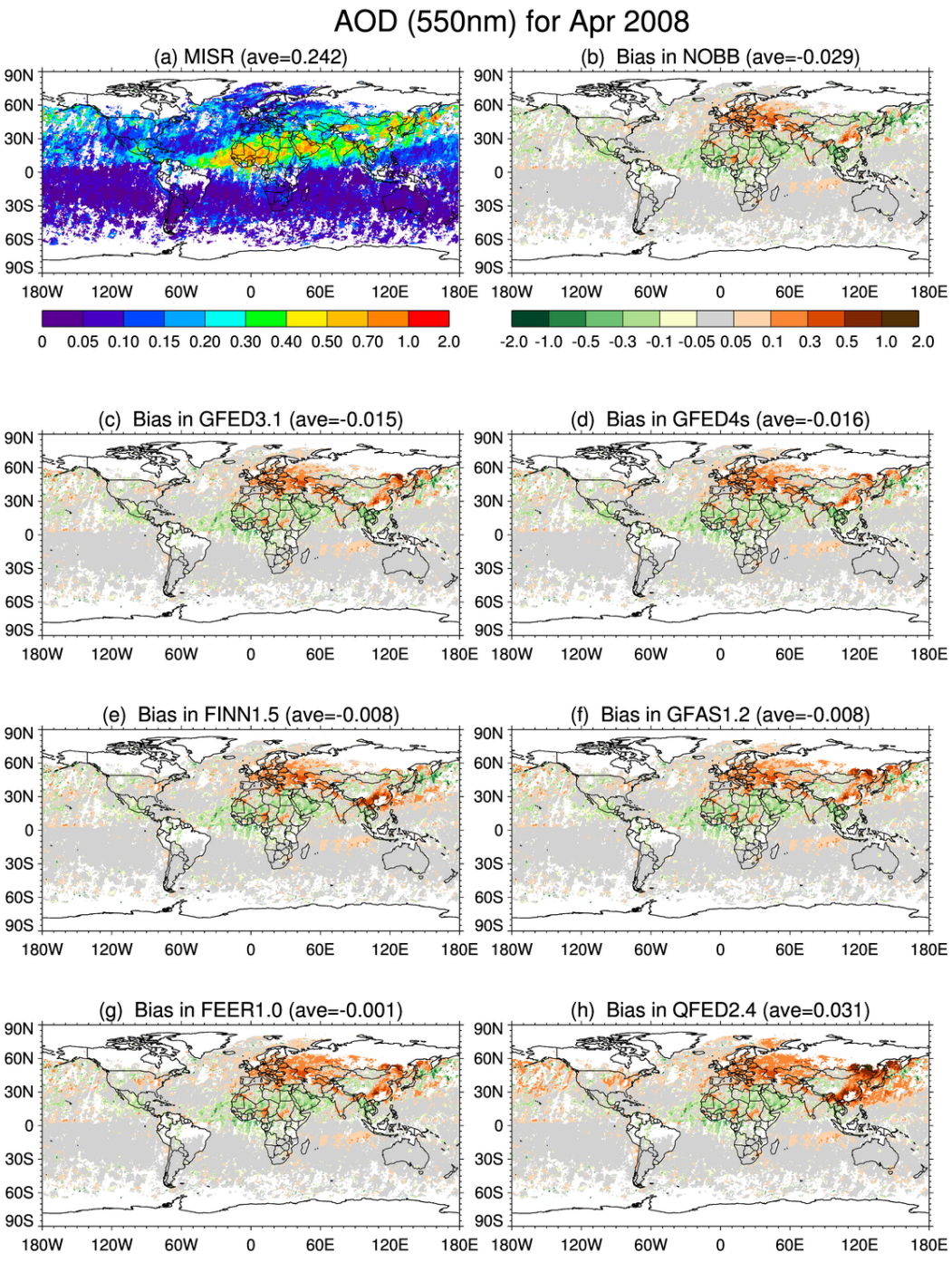

1417
1418 Figure 6. Same as Figure 5 except for April 2008.
1419

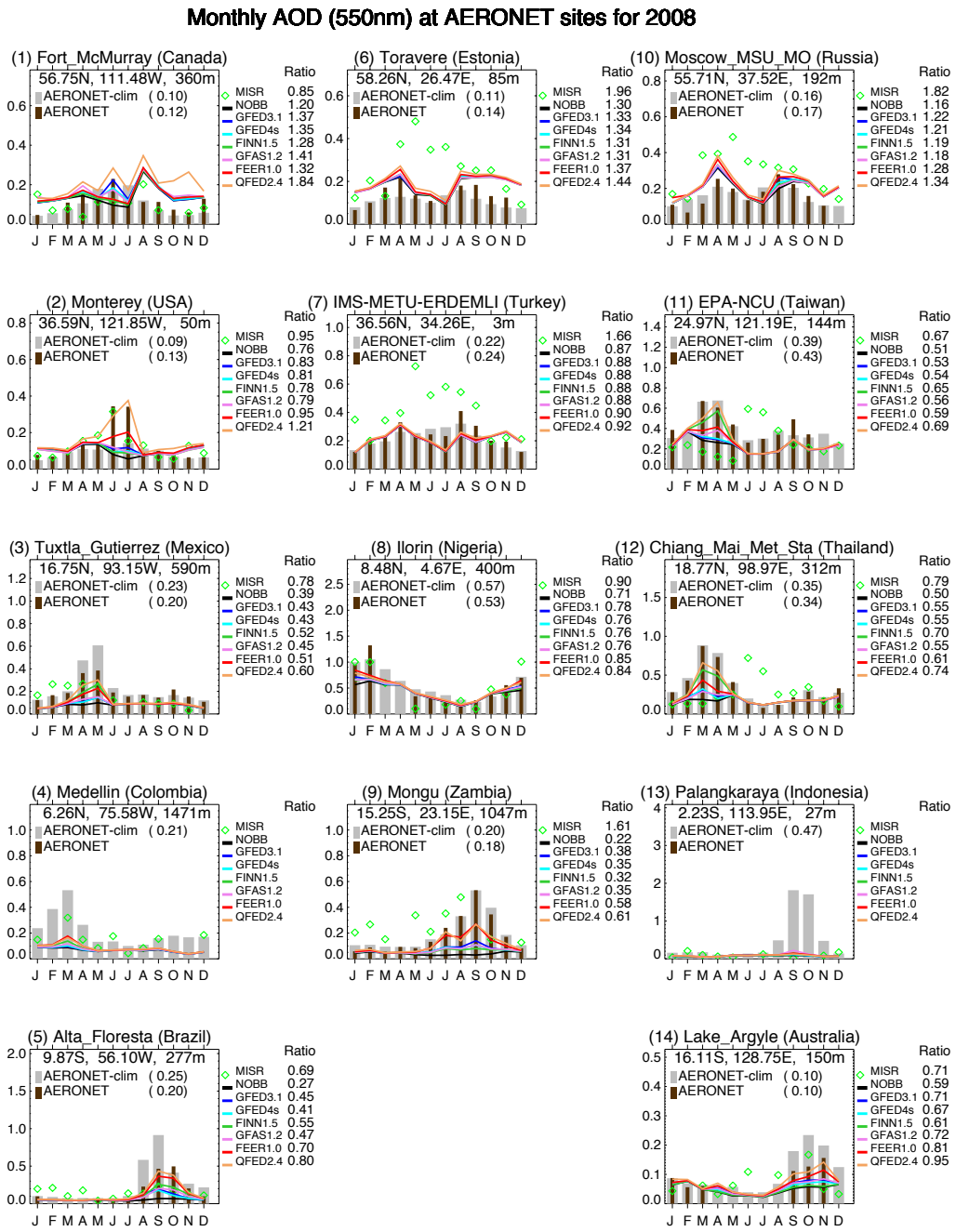

Figure 7. Monthly variation of AOD (at 550nm wavelength) for 2008 over 14 AERONET sites selected from the respective 14 regions (with its country indicated in parentheses). The climatology of AERONET AOD (i.e., AERONET-clim) is represented by light gray thick bars with yearly mean value shown in the parenthesis after its name, along with the monthly AERONET AOD represented by brown thin bars. MISR is represented by the green diamond, and seven GEOS experiments with different biomass burning emission options are represented by the lines in different colors. The annual ratio (Ratio=model/AERONET) listed on the right hand is estimated by averaging over monthly ratio.

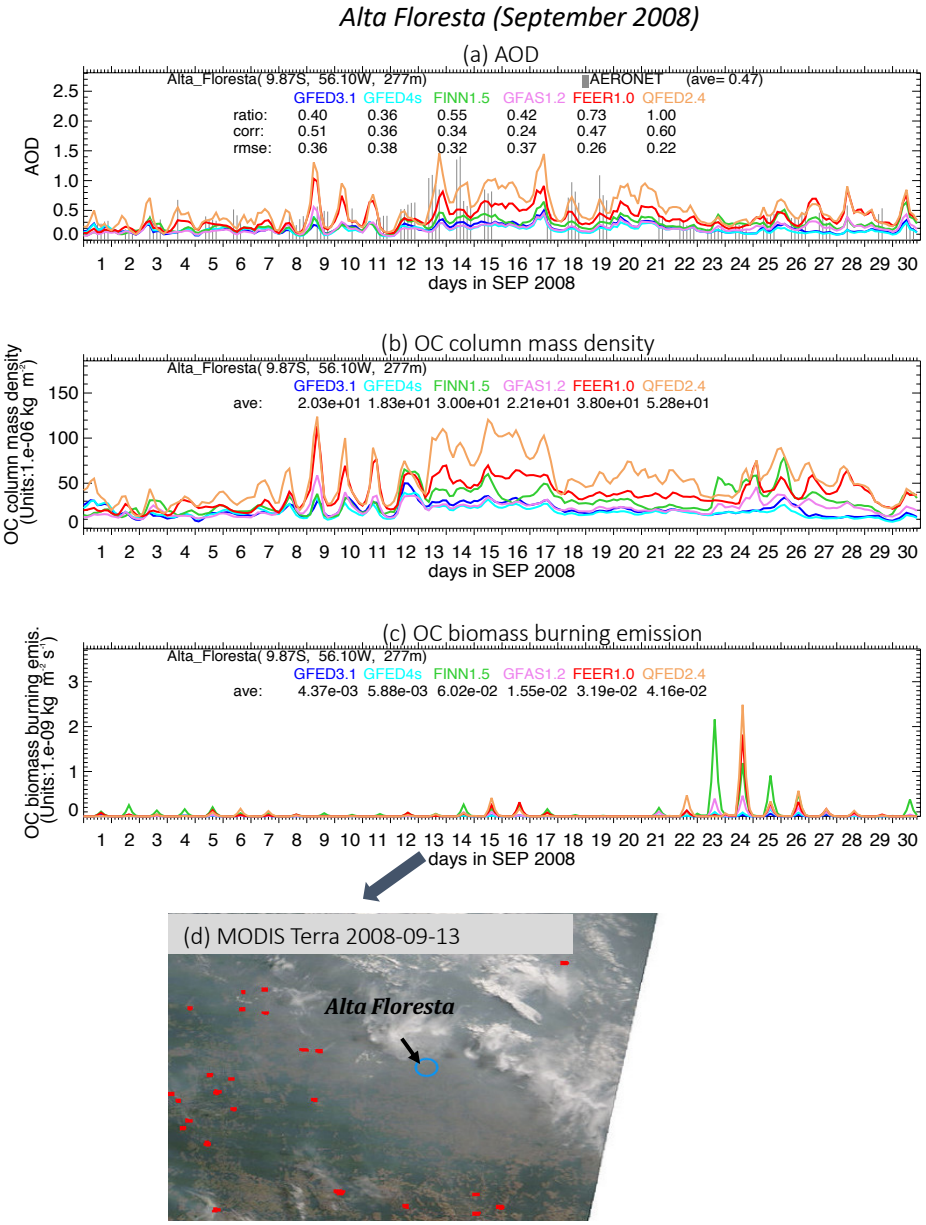

Figure 8. Characteristics of the observed and the simulated aerosols at Alta Floresta during September 2008: (a) The 3-hourly time series of AOD at 550nm. The AERONET is represented by vertical gray bars, and the outputs from the six model experiments are represented by the color curves. The relevant statistics are listed: *ave* is the monthly average, *ratio* is the fraction of the simulated to the observed AOD at all observed hours, *corr* is correlation between the observed and the simulated AOD, and *rmse* is root mean square error. (b) The 3-hourly time series of OC column mass density over the grid box where Alta Floresta is located (units: 1.e-06 kg m^{-2} or mg m^{-2}). (c) Same as (b) but biomass burning OC emission rate (units: 1.e-09 kg m^{-2} s^{-1} or μg m^{-2} s^{-1}). (d) MODIS-Terra true color image around Alta Floresta on September 13, 2008, overlaid with the active fire detections in red dots (Image credit: https://aeronet.gsfc.nasa.gov/cgi-bin/bamgomas_interactive and https://worldview.earthdata.nasa.gov).

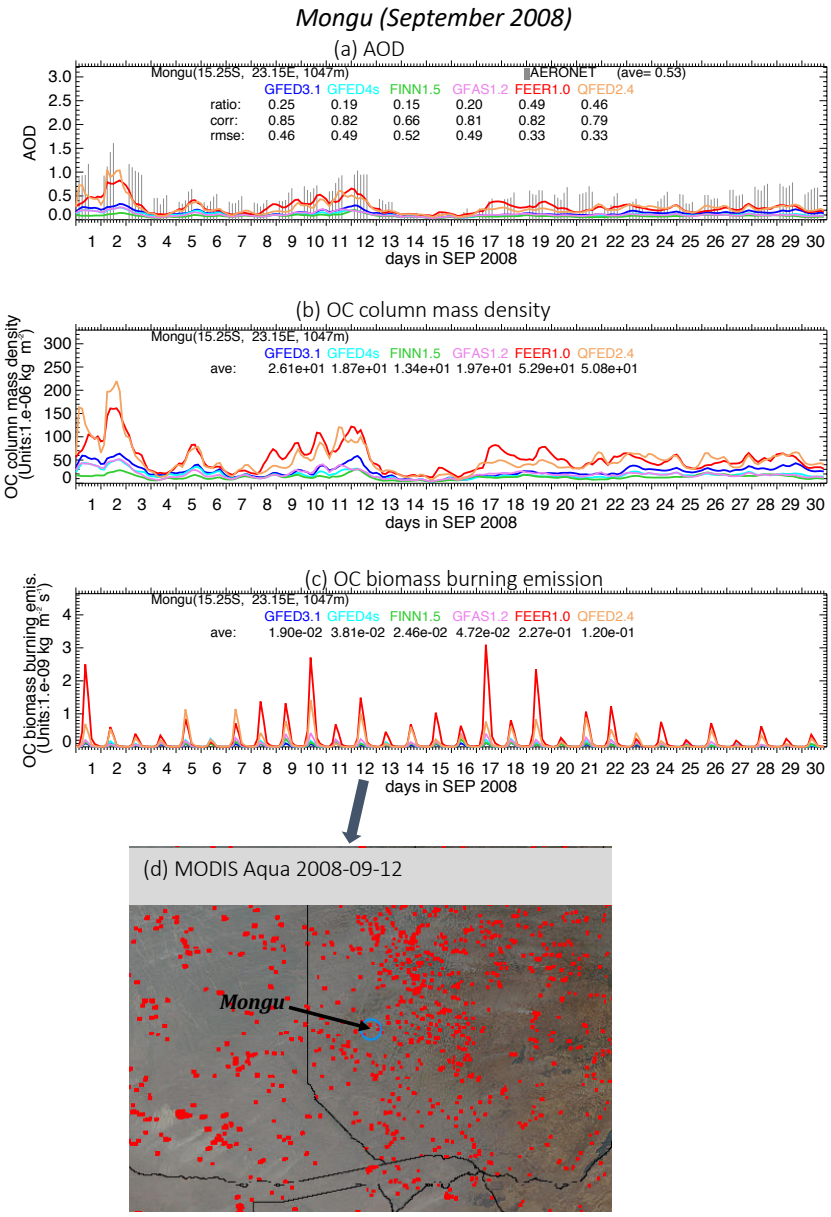

Figure 9. Characteristics of the observed and the simulated aerosols at Mongu during September 2008: (a) The 3-hourly time series of AOD at 550nm. The AERONET is represented by vertical gray bars, and the outputs from the six model experiments are represented by the color curves. The relevant statistics are listed: *ave* is the monthly average, *ratio* is the fraction of the simulated to the observed AOD at all observed hours, *corr* is correlation between the observed and the simulated AOD, and *rmse* is root mean square error. (b) The 3-hourly time series of OC column mass density over the grid box where Mongu is located (units: 1.e-06 kg m^{-2} or mg m^{-2}). (c) Same as (b) but biomass burning OC emission rate (units: 1.e-09 kg m^{-2} s^{-1} or μg m^{-2} s^{-1}). (d) MODIS-Aqua true color image around Mongu on September 12, 2008, overlaid with the active fire detections in red dots (Image credit: https://aeronet.gsfc.nasa.gov/cgi-bin/bamgomas_interactive and https://worldview.earthdata.nasa.gov).

1458 **Table 1.** Summary of six biomass burning emission datasets during MODIS-era (i.e., 2000-present)

a. Burned-area based approaches

BB Emission Dataset	Original Grid	Time-Frame/ Frequency	Burned Area	Active Fire Product	Fuel Consumption	Emission Factor
GFED3.1	0.5°×0.5° (lon×lat)	2000-2012/ 3-hourly, daily, monthly	MOD09GHK and/or MYD09GHK	Gridded composite L3 fire product MOD14A1 and/or MYD14A1	Estimated in CASA by product of fuel load and combustion completeness	Mainly from Andreae and Merlet (2001) with annual updates
GFED4s	0.25°×0.25° (lon×lat)	2000-2016/ 3-hourly, daily, monthly	Daily MCD64A1 product in Collection 5.1 at 500m spatial resolution	L3 MOD14A1 and MYD14A1; fire location product MCD14ML	Revised CASA by optimizing parameterization, reorientation of fuel consumption in frequently burned landscapes	Mainly from Akagi et al. (2011), supplemented by Andreae and Merlet (2001) and other
FINN1.5	1km^2	2002-2015/ daily	Estimated by active fire counts: 0.75 km^2 for savannas at each fire pixel, 1km^2 for other types	MODIS NRT active fire product (MCD14DL)	Assigned according to the global wildland fire emission model (Hoelzemann et al., 2004) with updates	Mainly from Andreae and Merlet (2001) and Akagi et al. (2011), with updates through 2015

1459

b. FRP based approaches

BB Emission Dataset	Original Grid	Time-Frame/ Frequency	FRP	Emission Coefficient (C_e)	Emission Factor
GFAS1.2	0.1×0.1 (lon×lat)	2003-Present/daily	Assimilation of level 2 MOD14 and MYD14 FRP	Calculated by regression of FRP to dry matter combustion rate of GFED v3.1 in 8 biomes.	Mainly from Andreae and Merlet (2001) with updates from literatures through 2009
FEER1.0	0.1×0.1 (lon×lat)	2003-Present/ daily, monthly	From GFASv1.2 (Kaiser et al., 2012, see above)	Calculated by linear regression between FRP and total particulate matter emission rate estimated from MODIS AOD at each grid	Andreae and Merlet (2001) with updates provided by Andreae in 2014
QFED2.4	0.1×0.1 (lon×lat)	2000-Present/ daily, monthly	Level 2 fire products MOD14/MYD14	Calculated by regression of the GEOS simulated AOD to the MODIS AOD in 46 sub-regions and then aggregated into 4 biomes.	Andreae and Merlet (2001)

1460 CASA: Carnegie-Ames-Stanford-Approach biogeochemical
1461

Table 2. Comparison of emission factor (Units: g species per kg dry matter burned) used by GFED3.1[1] and GFED4s[2] (listed in the upper and lower part of the cell respectively, bold if GFED4s is larger).

	Savanna and Grassland	Tropical Forest	Temperate Forest [3]	Boreal forest [3]	Peat Fires [4]	Agricultural Residues
OC	3.21 2.62	4.30 **4.71**	9.14 **9.60**	9.14 **9.60**	4.30 **6.02**	3.71 2.30
BC	0.46 0.37	0.57 0.52	0.56 0.50	0.56 0.50	0.57 0.04	0.48 **0.75**
SO_2	0.37 **0.48**	0.71 **0.40**	1.00 **1.10**	1.00 **1.10**	0.71 0.40	0.40 0.40
$PM_{2.5}$	4.94 **7.20**	9.05 **9.10**	12.84 **12.90**	12.84 **15.30**	9.05 **9.10**	8.25 6.30
CO_2	1646 **1686**	1626 **1643**	1572 **1647**	1572 1489	1703 1703	1452 **1585**
CO	61 **63**	101 93	106 88	106 **127**	210 210	94 **102**

[1.] Mainly from Andreae and Merlet (2001) with annual updates

[2.] Mainly from Akagi et al. (2011), supplemented by Andreae and Merlet (2001) and other sources

[3.] GFED4s (van der Werf et al., 2017) further divides extra-tropical forest in GFED3 (van der Werf et al., 2010) into temperate forest and boreal forest.

[4.] Based on Christian et al. (2003) for CO_2 and CO.